



Seasonality of aerosol optical properties in the Arctic

Lauren Schmeisser^{1,3,*}, John Backman², John A. Ogren^{1,3}, Elisabeth Andrews¹, Eija Asmi², Sandra Starkweather^{1,3}, Taneil Uttal³, Markus Fiebig⁴, Sangeeta Sharma⁵, Kostas Eleftheriadis⁶, Stergios Vratolis⁶, Michael Bergin⁷, Peter Tunved⁸, and Anne Jefferson¹

¹University of Colorado, Cooperative Institute for Research in Environmental Sciences, Boulder, CO, USA

²Finnish Meteorological Institute, Atmospheric Composition Research, Helsinki, Finland

³National Oceanic and Atmospheric Administration, Earth System Research Laboratory, Boulder, CO, USA

⁴Norwegian Institute for Air Research, Kjeller, Norway

⁵Environment and Climate Change Canada, Science & Technology Branch, Climate Research Division, Toronto, Canada

⁶Institute of Nuclear and Radiological Science & Technology, Energy & Safety, Environmental Radioactivity Laboratory, NCSR Demokritos, Athens, Greece

⁷Duke University, Department of Civil & Environmental Engineering, Durham, NC, USA

⁸Stockholm University, Department of Environmental Science and Analytical Chemistry, Stockholm, Sweden

* now at: University of Washington, Department of Atmospheric Sciences, Seattle, WA, USA

Correspondence: Lauren Schmeisser (lauren.schmeisser@gmail.com)

Received: 1 December 2017 – Discussion started: 31 January 2018

Revised: 12 July 2018 – Accepted: 26 July 2018 – Published: 16 August 2018

Abstract. Given the sensitivity of the Arctic climate to short-lived climate forcers, long-term in situ surface measurements of aerosol parameters are useful in gaining insight into the magnitude and variability of these climate forcings. Seasonality of aerosol optical properties – including the aerosol light-scattering coefficient, absorption coefficient, single-scattering albedo, scattering Ångström exponent, and asymmetry parameter – are presented for six monitoring sites throughout the Arctic: Alert, Canada; Barrow, USA; Pallas, Finland; Summit, Greenland; Tiksi, Russia; and Zeppelin Mountain, Ny-Ålesund, Svalbard, Norway. Results show annual variability in all parameters, though the seasonality of each aerosol optical property varies from site to site. There is a large diversity in magnitude and variability of scattering coefficient at all sites, reflecting differences in aerosol source, transport, and removal at different locations throughout the Arctic. Of the Arctic sites, the highest annual mean scattering coefficient is measured at Tiksi (12.47 Mm^{-1}), and the lowest annual mean scattering coefficient is measured at Summit (1.74 Mm^{-1}). At most sites, aerosol absorption peaks in the winter and spring, and has a minimum throughout the Arctic in the summer, indicative of the Arctic haze phenomenon; however, nuanced variations in seasonalities suggest that this phenomenon is not

identically observed in all regions of the Arctic. The highest annual mean absorption coefficient is measured at Pallas (0.48 Mm^{-1}), and Summit has the lowest annual mean absorption coefficient (0.12 Mm^{-1}). At the Arctic monitoring stations analyzed here, mean annual single-scattering albedo ranges from 0.909 (at Pallas) to 0.960 (at Barrow), the mean annual scattering Ångström exponent ranges from 1.04 (at Barrow) to 1.80 (at Summit), and the mean asymmetry parameter ranges from 0.57 (at Alert) to 0.75 (at Summit). Systematic variability of aerosol optical properties in the Arctic supports the notion that the sites presented here measure a variety of aerosol populations, which also experience different removal mechanisms. A robust conclusion from the seasonal cycles presented is that the Arctic cannot be treated as one common and uniform environment but rather is a region with ample spatiotemporal variability in aerosols. This notion is important in considering the design of aerosol monitoring networks in the region and is important for informing climate models to better represent short-lived aerosol climate forcers in order to yield more accurate climate predictions for the Arctic.

1 Introduction

The Arctic is a unique environment, characterized by sensitive interactions and feedbacks between the atmosphere, ocean, cryosphere, and biosphere (Serreze and Francis, 2006; Serreze and Barry, 2011). In recent decades, substantial changes have been observed in the Arctic, including increases in air temperature (Johannessen et al., 2004), decreases in sea ice extent and thickness (Lindsay and Zhang, 2005; Stroeve et al., 2007, 2012), changes in Arctic vegetation (Wang and Overland, 2004; Chapin et al., 2005; Pearson et al., 2013), and shifts in precipitation patterns (Groves and Francis, 2002; Bintanja and Selten, 2014). The mechanisms behind these changes are induced by anthropogenic global climate change (Anisimov et al., 2007) and have not yet been fully characterized. Human presence and thus emissions in the Arctic are likely to increase in the future due to decreases in sea ice making the region more accessible for energy extraction and shipping activities (e.g., Aliabadi et al., 2015; Eckhardt et al., 2013). More research in the Arctic, particularly on atmospheric components and processes in the region, is necessary to better understand what is changing, why it is changing, and how it might change in the future (Anisimov et al., 2007).

Within the Arctic atmosphere, short-lived climate forcers like aerosols are important contributors to the observed warming and environmental changes in the region (Quinn et al., 2008; Najafi et al., 2015). Aerosols can affect the climate both directly by scattering and absorbing incoming solar radiation and indirectly through aerosol–cloud interactions (Twomey, 1977). Quantifying the forcing by aerosols in the Arctic is especially complex, given the annual variability in surface albedo and cloudiness, the stratified atmosphere, resulting feedbacks, and long-range aerosol transport. Measurements of surface Arctic aerosol optical properties in particular can help define and constrain interannual, seasonal, and diurnal variability of light scattering and absorption, potential particle sources, and resulting radiative forcing. The observation capacity demonstrated here has potential for providing *in situ* observational checks on long-term black carbon inventories and monitoring strategies of importance to international pollution mitigation effects. This paper will seek to provide an overview of surface aerosol optical properties in the Arctic.

2 Background

Observations of aerosols in the Arctic have a long (>50 years) history (e.g., Mitchell's, 1957, report on so-called Arctic haze layers), although continuous surface measurements of aerosol optical properties did not begin until the mid-1970s at Barrow, Alaska (BRW), and later at other sites. The start of long-term, continuous surface measurements, ongoing to this day, have provided information about

aerosol chemistry, microphysics, and optical properties and enabled the development of aerosol climatologies, the analysis of trends, and the evaluation of models. Such analyses have been driven by the need to understand the remote and local sources, transport, and processes that influence aerosol properties in the Arctic. Understanding aerosol optical properties in particular is important in gaining insight into the role of aerosols in the Arctic's radiative energy budget (e.g., Quinn et al., 2011).

Despite the challenges associated with performing high-quality, long-term atmospheric observations in the Arctic (e.g., high costs, extreme conditions, difficult access), several monitoring stations do currently exist in the Arctic. Of these monitoring sites, 10 contribute to the International Arctic Systems for Observing the Atmosphere (IASOA) network. The purpose of the IASOA organization is twofold: (1) to enhance interoperable observational abilities and coverage of surface atmospheric monitoring in the data-sparse Arctic, and (2) to foster pan-Arctic scientific collaboration with easier data access and strengthened synergy among researchers (Uttal et al., 2016). Of the 10 monitoring sites, six stations have multi-year, continuous measurements of aerosol optical properties, and it is these data from 2012 to 2014 that are used for the Arctic aerosol analysis presented in this paper. These monitoring stations follow standardized aerosol sampling protocol, as advised by the Global Atmosphere Watch (GAW) network (http://library.wmo.int/opac/index.php?lvl=notice_display&id=19622, last access: 1 October 2017), and contribute to a coordinated data archive (i.e., the World Data Centre for Aerosols (WDCA) hosted at the Norwegian Institute for Air Research, <http://ebas.nilu.no/>, last access: 13 November 2016).

Published climatologies and seasonality of surface extensive aerosol optical properties (i.e., properties that depend on the amount of aerosol) have shown that, at many Arctic sites, scattering and absorption are highest in the late winter and early spring, and lowest in the summer (e.g., Bodhaine, 1983 (Barrow); Bodhaine, 1995 (Barrow); Sharma et al., 2004 (Alert); Eleftheriadis et al., 2009 (Zeppelin); Heintzenberg, 1982 (Zeppelin); Aaltonen et al., 2006 (Pallas); Lihavainen et al., 2015 (Pallas)). However, results shown here will support the notion that not all Arctic sites have this seasonal cycle. The winter/spring aerosol enhancement is called Arctic haze, referring back to Mitchell's (1957) early airborne observations. Understanding the sources, characteristics, and effects of Arctic haze has been a continuing effort over the past several decades (e.g., Rahn et al., 1977; Shaw, 1995; Quinn et al., 2007; Liu et al., 2015; and references therein). The low summertime values of absorption and scattering currently observed in the Arctic are likely to be particularly vulnerable to warmer, drier climatic conditions (e.g., due to increases in summertime forest fires and decreases in sea ice leading to enhanced marine emissions and human activities in the region during the summer). Published climatologies and seasonal cycles of *in situ* Arctic intensive aerosol prop-

erties (i.e., properties that are ratios of extensive properties and not directly dependent on aerosol amount) are sparse and suggest that, unlike the relatively consistent seasonal pattern for extensive properties, the seasonal cycles of intensive optical properties (e.g., Ångström exponent) may differ from site to site (Delene and Ogren, 2002; Aaltonen et al., 2006; Lihavainen et al., 2015). This work seeks to expand on previous aerosol optical analyses in the Arctic by synthesizing aerosol seasonality at multiple Arctic stations and adding new knowledge on the seasonality of intensive aerosol characteristics in the region.

At present, only surface measurements can provide a seasonal context for the range of aerosol optical properties used to determine radiative forcing efficiency (RFE), including absorption, scattering, backscattering fraction, asymmetry parameter, and single-scattering albedo. While vertical profiles are important due to the stratified conditions in the Arctic atmosphere (e.g., Rahn et al., 1977), aircraft campaigns in the Arctic thus far do not provide insight into seasonality. Stone et al. (2014; their Fig. 5) note that only one aircraft campaign in the last 30 years occurred outside the Arctic haze period. Remote-sensing instruments such as sun photometers are limited due to long periods of darkness during the winter, and satellite measurements have limited utility due to the high albedo of the Arctic snow surface and the dark Arctic winters. An additional limitation of remote-sensing measurements is that parameters important for RFE calculations (e.g., single-scattering albedo) cannot be retrieved without high uncertainties in the Arctic due to the low aerosol optical depth (AOD) (Dubovik et al., 2000). Although geographically sparse compared to the potential of remote-sensing and aircraft campaigns, surface measurements have the advantage of being long-term, year-round, and comprehensive.

The objective of this paper is to explore the seasonality and spatiotemporal variability of surface aerosol optical properties in the Arctic; the results of this exploration may be useful for continued improvement of modeling and remote-sensing capabilities. Here we ask how aerosol optical properties differ among six Arctic monitoring sites, how monthly variability in aerosol optical properties compares across the sites, what systematic variability among aerosol optical properties exists in the Arctic, what pairing of trajectory data with aerosol optical properties suggests about aerosol sources in the Arctic, and how this trajectory analysis varies geographically from station to station.

3 Methods

3.1 Monitoring sites

The analysis presented here uses in-situ-measured aerosol properties from six Arctic monitoring stations. To be included in the analysis, a station had to have continuous and concurrent aerosol light scattering and two sets of absorp-

tion measurements: (i) Aethalometer and (ii) “reference” co-located absorption instrument (details in Sect. 3.2) during years 2012–2014. Six monitoring sites met these criteria: Alert, Canada (ALT); Barrow, Alaska (BRW); Pallas, Finland (PAL); Summit, Greenland (SUM); Tiksi, Russia (TIK); and Zeppelin Mountain, Ny-Ålesund, Svalbard, Norway (ZEP) (for a record of data availability at all IASOA sites, see the IASOA data access portal: <https://www.esrl.noaa.gov/psd/iasoa/dataataglance>, last access: 1 July 2018). The following sections describe the location of, conditions at, and instrumentation at the sites analyzed here. Arctic stations not included in this study either do not measure the parameters presented here or do not have continuous measurements for the period of interest. This time period was chosen to align with Backman et al. (2017), who present an Arctic-specific correction scheme for Aethalometer data, to be used here to describe absorption coefficients at each of the stations. More information on this correction scheme is presented in Sect. 3.2. Table 1 provides further information on monitoring station location, instrumentation, and sampling inlet configuration. Figure 1 shows a map of the Arctic sites, as well as photos of the monitoring stations and their surroundings.

3.1.1 Alert, Canada (ALT)

Alert is located in Nunavut, Canada, and is operated by Environment and Climate Change Canada (ECCC). The aerosol optical property measurements are made in collaboration with the National Oceanic and Atmospheric Administration (NOAA). The monitoring station is the most northerly site in the GAW network; despite the site being shared with a Canadian military facility and an ECCC upper-air weather station, it is remote and far from industrial pollution sources. The measurement laboratory was established in 1986 and has long-term Aethalometer measurements from 1989 on and aerosol absorption (particle soot absorption photometer, or PSAP) and scattering measurements from 2005 on. The aerosol instruments measure from an inlet and aerosol system that has both 1 and 10 µm diameter size cuts, and data from the 10 µm size cut are used here. Relative humidity (RH) of the sample is consistently less than 40 %, which is important in limiting effects of hygroscopic growth on the aerosol measurements. Instrument descriptions can be found in Table 1. Previous work on aerosol optical properties at ALT can be found in Hopper et al. (1994), Sharma et al. (2002, 2004, 2006), and Quinn et al. (2007).

3.1.2 Barrow, Alaska (BRW)

The Barrow observatory was established in 1973 and is operated by NOAA with additional support from the U.S. Department of Energy and the National Science Foundation (NSF). The site is situated 5 km northeast of the town of Barrow, Alaska (population: ~4200), and is 2 km from the

Table 1. Monitoring station names, locations, scattering and absorption instruments, size cuts, and humidity of samples. Bolded instruments indicate those from which data are used in this analysis.

Station code and location	Latitude longitude elevation	scattering instrument(s) [size cut]	Co-located absorption photometer instrument(s) [size cut]	Aethalometer model(s) [size cut]	RH of sample
ALT Alert, Canada	82.49915° N 62.34153° W 210 m a.s.l.	<i>2004–present:</i> nephelometer 3563 ¹ [10 µm]	<i>2004–2010:</i> PSAP-1W ³ <i>2007–present:</i> PSAP-3W ⁵ [10 µm]	<i>1989–2009:</i> Aethalometer AE6 ⁸ <i>2008–present:</i> Aethalometer AE31 ¹⁰ [none]	< 40 %
BRW Barrow, Alaska	71.32301° N 156.6115° W 11 m a.s.l.	<i>1976–1997:</i> nephelometer 1559B ² <i>1997–present:</i> nephelometer 3563 ¹ [10 µm]	<i>1997–2006:</i> PSAP-1W ³ <i>2006–present:</i> PSAP-3W ⁵ <i>2011–present:</i> CLAP ⁶ [10 µm]	<i>1988–2002:</i> Aethalometer AE8 ⁹ <i>2010–present:</i> Aethalometer AE31 ¹⁰ [10 µm] <i>2014–present:</i> Aethalometer AE33 ¹¹	< 40 %
PAL Pallas, Finland	67.97361° N 24.11583° E 560 m a.s.l.	<i>2000–present:</i> nephelometer 3563 ¹ [2.5 µm]	<i>2007–present:</i> MAAP ⁷ [2.5 µm]	<i>2005–present:</i> Aethalometer AE31 ¹⁰ [none]	< 40 %
SUM Summit, Greenland	72.58000° N 38.48000° W 3238 m a.s.l.	<i>2011–present:</i> nephelometer 3563 ¹ [2.5 µm]	<i>2011–present:</i> CLAP ⁶ [2.5 µm]	<i>2003–present:</i> Aethalometer AE16 ¹² [2.5 µm] <i>2014–present:</i> Aethalometer AE33 ¹¹	< 40 %
TIK Tiksi, Russia	71.58617° N 128.91882° E 8 m a.s.l.	<i>2013–present:</i> nephelometer 3563 ¹ [10 µm]	<i>2013–present:</i> MAAP ⁷ [10 µm]	<i>2009–present:</i> Aethalometer AE31 ¹⁰ [10 µm]	< 30 %
ZEP Zeppelin Mountain, Ny-Ålesund, Norway	78.90669° N 11.88934° E 475 m a.s.l.	<i>2010–present:</i> nephelometer 3563 ¹ [none]	<i>2002–present:</i> PSAP-1W ⁴ [none]	<i>2005–present:</i> Aethalometer AE31 ¹⁰ [none]	< 20 %

¹ TSI nephelometer 3563. ² MRI nephelometer 1559B. ³ Radiance Research one-wavelength particle soot absorption photometer (PSAP-1W). ⁴ Custom-built one-wavelength particle soot absorption photometer (PSAP-1W). ⁵ Radiance Research three-wavelength particle soot absorption photometer (PSAP-3W). ⁶ NOAA Continuous Light Absorption Photometer (CLAP). ⁷ Thermo Fisher Scientific Multi-angle Absorption Photometer (MAAP) Model 5012. ⁸ Magee Aethalometer AE6. ⁹ Magee Aethalometer AE8. ¹⁰ Magee Aethalometer AE31. ¹¹ Magee Aethalometer AE33. ¹² Magee Aethalometer AE16.

Arctic Ocean coast. The station primarily measures regionally representative air masses coming off of the Beaufort Sea. Air masses coming from the direction of the town are marked as contaminated, and those data are not used here. Aerosols are sampled through an inlet and aerosol system with a switching impactor that has both 1 and 10 µm size cuts, though only data from the 10 µm size cut are analyzed here. The Aethalometer samples air from a separate inlet with no aerosol size cut and thus measures the full aerosol size range. Previous descriptions of the aerosol optical property climatology from the older generation of instrumentation at BRW (see Table 1) are found in Bodhaine (1983, 1995), Delene and Ogren (2002), and Quinn et al. (2007).

3.1.3 Pallas, Finland (PAL)

The Pallas Atmosphere-Ecosystem Supersite is operated by the Finnish Meteorological Institute (FMI) and is a part of the larger Pallas-Sodankylä GAW station located in northern Finland. The Pallas main research site is located in the Pallas-Yllästunturi National Park on the top of the Sammal-tunturi fell at an elevation of 565 m a.s.l. and above the tree line. The nearest town is Muonio, located 19 km to the west with ~2500 inhabitants, though the station typically measures clean Arctic air masses due to a prevailing wind direction not affected by town contamination. The surrounding region is hilly and vegetated with pine, spruce, birch, and low-growing shrubs. The total aerosol inlet at PAL is slightly heated to avoid freezing and to maintain RH below 40 %. The Aethalometer is connected to the total aerosol in-

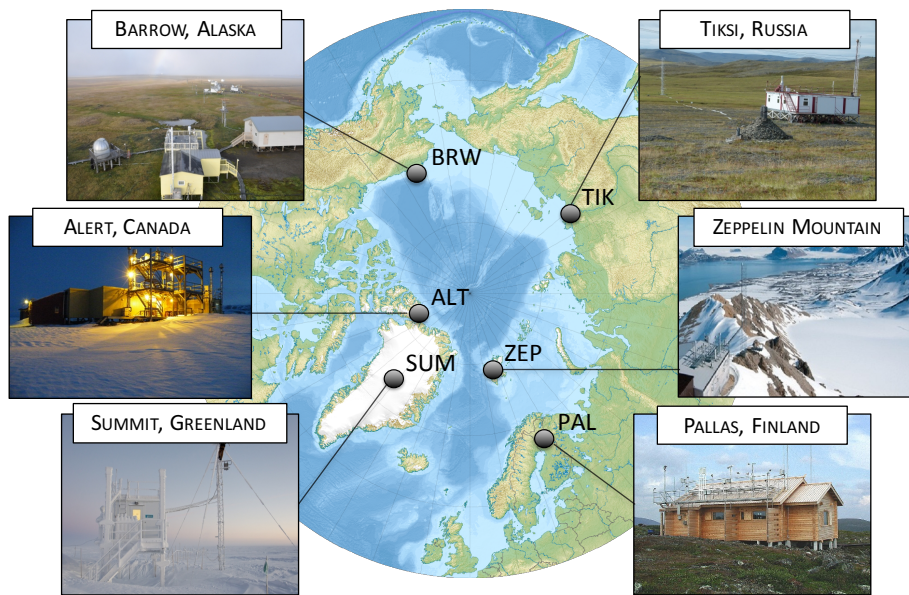


Figure 1. Map of Arctic monitoring stations with pictures of each site.

let. The other optical measurements (Multi-angle Absorption Photometer (MAAP) and nephelometer) are connected to a $10\text{ }\mu\text{m}$ size cut inlet. A more detailed description of aerosol optical measurements and sampling can be found in Lihavainen et al. (2015) and in Backman et al. (2017). A climatology of aerosol optical properties at PAL is presented by Aaltonen et al. (2006) and Lohila et al. (2015).

3.1.4 Summit, Greenland (SUM)

The Summit monitoring station is located in Greenland, Denmark, and is supported and operated by Duke University in collaboration with NOAA Earth Systems Research Laboratory with financial aid from the NSF. The scattering and co-located absorption measurements at SUM were initiated in 2011 as part of a NOAA collaboration with the Georgia Institute of Technology. Summit is unique from the other stations in this study due to its high elevation of 3238 m a.s.l., meaning it often measures free-tropospheric air. The station is very remote and has no nearby anthropogenic aerosol sources apart from scientific operations near the site; when air masses blow from the direction of the scientific camp, data are marked as contaminated and are not included in this analysis. The inlet at Summit has a $2.5\text{ }\mu\text{m}$ size cut, and samples have $\text{RH} < 40\text{ }%$, since the temperature inside the instruments is much warmer than the temperature outside. Van Curen et al. (2012) has some description of past aerosol measurements made at SUM.

3.1.5 Tiksi, Russia (TIK)

The Tiksi Hydrometeorological Observatory in Yakutsk, Russia, was formed through a collaboration between the Rus-

sian Federal Services for Hydrometeorological and Environmental Monitoring (Roshydromet), NOAA, FMI, and NSF. Though there has been a meteorological observatory at this location since the 1930s, the new international site was established in 2009. The site is located in northern Siberia in the Sakha Republic of Russia, just 500 m from the coast of the Laptev Sea and ~ 5 km outside of the town of Tiksi (population: 4600). Air masses coming from the direction of the town are marked as contaminated and are not included in this analysis. The monitoring station is surrounded by a tundra landscape, as seen in the photo of the Tiksi monitoring site in Fig. 1. Air is sampled through a heated inlet that prevents ice buildup and minimizes hygroscopic effects on the measurements by keeping $\text{RH} < 40\text{ }%$, and it has a $10\text{ }\mu\text{m}$ size cut. A detailed description of the Tiksi site can be found in Uttal et al. (2013), and a previous analysis of aerosols at TIK with a detailed description of the sampling system can be found in Asmi et al. (2016).

3.1.6 Zeppelin Mountain, Ny-Ålesund, Norway (ZEP)

The Zeppelin Mountain observatory is located on a small mountain at 475 m a.s.l., just south of the small research village of Ny-Ålesund (30–150 inhabitants, depending on time of year) on Svalbard in Norway. The monitoring station is owned by the Norwegian Polar Institute and operated by the Norwegian Institute for Air Research (NILU), and the most recent version of the station building was constructed in the year 2000. The site is typically located above the inversion layer and thus measures air masses with minimal contamination. Aerosol instruments sample from an inlet line that reaches room temperature ($\sim 21\text{ }^\circ\text{C}$) before measurement so that $\text{RH} < 20\text{ }%$. The inlet line does not have a size cut. Past

analyses of aerosol measurements at ZEP can be found in Ström et al. (2003), Stohl et al. (2006b), and Eleftheriadis et al. (2009).

3.2 Data and instrumentation

Although monitoring networks offer scientists an opportunity for regional cross-station analyses of aerosol seasonality and climatologies, comparing data across monitoring sites requires caution. Care must be taken to ensure data are measured, edited, and corrected using comparable high-quality methods. Moreover, comparing the same aerosol property measured by different instrument types or models necessitates extra attention. This section describes the data and steps taken to ensure comparability of those data for this analysis.

All six sites in this analysis have scattering measurements for years 2012–2014 from an integrating nephelometer (TSI model 3563) measuring at three wavelengths (450, 550, 700 nm). Corrections to the raw scattering coefficient measurements are necessary to account for light source and angular non-idealities, and the correction methods described in Anderson and Ogren (1998) were used to correct the scattering coefficient data presented here.

In this analysis, absorption data are available from Aethalometers as well as other co-located filter-based absorption instruments (i.e., Continuous Light Absorption Photometer (CLAP), PSAP, and/or MAAP) at each observatory. The Magee Aethalometers are the only common absorption instrument among the six stations presented here, and this paper synthesizes the absorption data from Aethalometers across the Arctic. The Aethalometer data are corrected using the new Arctic-specific Aethalometer correction scheme presented by Backman et al. (2017). We use the reference co-located absorption instruments to gauge whether the corrected Aethalometer data are similar to what is expected for absorption coefficient values from other absorption measurements at the stations. The different co-located absorption instruments and Aethalometer data are described below.

Co-located reference absorption data at ALT are from a Radiance Research three-wavelength (467, 530, 660 nm) particle soot absorption photometer (PSAP-3W) and at ZEP are from a custom-built one-wavelength (525 nm) particle soot absorption photometer (PSAP-1W). The PSAP collects aerosol particles on a filter and relates the change in light transmission through the filter over time to the absorption coefficient of the deposited aerosol. PSAP data are corrected using the correction schemes from Bond et al. (1999) and Ogren (2010) to adjust for multiple-scattering effects, filter loading, apparent absorption, flow bias, spot size bias, and spectral scattering. Correcting for apparent absorption requires concurrent measurements of aerosol light scattering, which are available from TSI nephelometers at all six stations.

Co-located absorption data at BRW and SUM were measured using a CLAP at three wavelengths (467, 528, 652 nm).

The CLAP is an instrument designed and built by NOAA that is based on the PSAP design, except that it samples consecutively on eight filter spots on one large 47 mm filter, as opposed to the one spot available on the 10 mm PSAP filter. The CLAP's multi-spot functionality enables it to run unattended for 8 times longer than the PSAP, making it ideal for remote, less frequently visited locations (Ogren et al., 2017). The CLAP data are corrected the same way as the PSAP using Bond et al. (1999) and Ogren (2010) corrections.

PAL and TIK co-located reference absorption data are from a Thermo Fisher Scientific MAAP at one wavelength (637 nm) (Müller et al., 2011). The MAAP is a filter-based absorption instrument that measures filter transmittance as well as backscattered light at two angles (Petzold and Schönlinner, 2004). The backscattering measurements at different angles allow the instrument to account for multiple-scattering and apparent absorption effects. Due to the low concentrations in the Arctic, no post-processing corrections are needed (Hyvärinen et al., 2013).

In addition to the co-located absorption measurement, all monitoring stations have absorption data collected from some model of the Magee Aethalometer. During 2012–2014, five of the stations – ALT, BRW, ZEP, PAL, and TIK – operated a seven-wavelength (370, 470, 520, 590, 660, 880, and 950 nm) Aethalometer AE31, while SUM operated a one-wavelength (880 nm) Aethalometer AE16. The Aethalometer measures light transmitted through a filter on which particles are deposited and interprets the change in transmittance, or the attenuation of light through the filter, as the aerosol light absorption, which the instrument reports as an atmospheric concentration of equivalent black carbon (eBC) (Petzold et al., 2013) particles using a mass absorption cross section of black carbon. There are known artifacts associated with measuring absorption coefficients on the Aethalometer filter tape, including multiple scattering by filter fibers, scattering by aerosol deposited on the filter, and decrease in sensitivity with increased filter loading. Many Aethalometer correction schemes exist that try to account for one or all of these artifacts (e.g., Collaud Coen et al., 2010; Drinovec et al., 2015), including GAW recommendations for the AE31 contained in GAW report 227 (https://library.wmo.int/opac/docnum.php?explnum_id=3073, last access: 1 August 2018), but there is currently no agreed-upon or widely accepted correction scheme. Here we use a new Arctic-specific Aethalometer correction factor from Backman et al. (2017) to derive the light absorption coefficient from the Aethalometer data.

Backman et al. (2017) present an Arctic-specific multiple-scattering enhancement factor, C_f , derived from Aethalometer data and co-located absorption data from the same sites and time period used in this study. For all wavelengths and for the five low-altitude sites (ALT, BRW, PAL, TIK, ZEP), the value for C_f was found to be 3.45, with interquartile values of 2.93–4.15. The Arctic correction factor is used to cor-

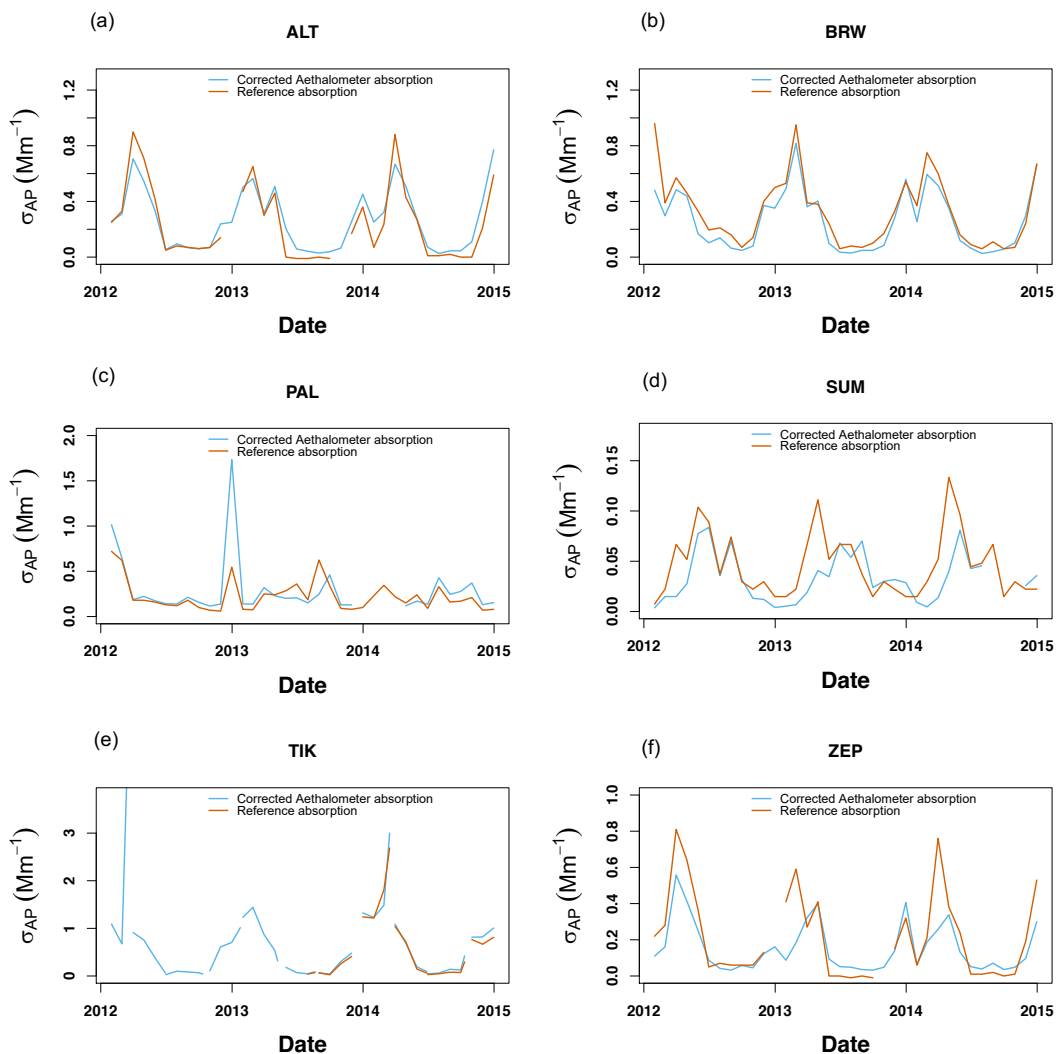


Figure 2. Comparison of monthly medians (computed from hourly data) and corrected Aethalometer absorption (light blue) and absorption measured by co-located absorption instrument (orange). (a) ALT absorption at 467 nm, (b) BRW absorption at 467 nm, (c) PAL absorption at 637 nm, (d) SUM absorption at 880 nm, (e) TIK absorption at 637 nm, (f) ZEP absorption at 525 nm. All data are at wavelength of co-located absorption instrument (PSAP, CLAP, or MAAP) except for SUM, where data are at wavelength of the one-wavelength AE16 Aethalometer (880 nm). Note that y axes are different on each plot.

rect Aethalometer data using Eq. (1):

$$C_f = \frac{\sigma_o}{\sigma_{ap}}, \quad (1)$$

where σ_o is the uncorrected Aethalometer absorption coefficient and σ_{ap} is the actual absorption coefficient that is corrected for multiple scattering by the filter fibers. Note that this correction scheme does not consider scattering by particles deposited on the Aethalometer filter or sensitivity of measurements to Aethalometer filter loading.

The Aethalometer absorption data corrected with the Backman et al. (2017) correction factor are compared to absorption coefficients from the co-located absorption instruments to ensure that the corrected Aethalometer data are sim-

ilar to absorption coefficients that are measured by other absorption instruments at the site. Figure 2 shows a time series of monthly median corrected Aethalometer data and co-located absorption data from 2012 to 2014 at each site. Data are adjusted to a co-located absorption instrument wavelength, except for SUM data, where the co-located absorption data are adjusted to the wavelength of the one-wavelength Aethalometer (880 nm). Wavelengths of the data in Fig. 2 are 467 nm at ALT, 467 nm at BRW, 637 nm at PAL, 880 nm at SUM, 637 nm at TIK, and 525 nm at ZEP. Note that the y-axis scales in Fig. 2 are different for each site. Additional scatterplots comparing Aethalometer and co-located absorption data, including R^2 values, can be found in the Supplement. In general, the corrected Aethalometer absorption co-

efficients compare well to the co-located absorption coefficients, though the comparability differs with season and site. ALT and BRW show good agreement between both absorption coefficient datasets ($R^2 = 0.809$ for ALT, $R^2 = 0.839$ for BRW) throughout the entire time. At BRW, there is a small systematic bias such that the co-located absorption values are slightly higher than the corrected Aethalometer absorption values. PAL also shows good agreement ($R^2 = 0.779$) between absorption measurement techniques for the given time, apart from January 2013, which does not compare as well as the other months. Review of the PAL data revealed no immediately apparent problems that could explain the anomalous results in January 2013. SUM has the worst agreement between co-located absorption data and corrected Aethalometer absorption data ($R^2 = 0.384$), with higher biases in the winter and spring, and better agreement in the datasets in the summer. SUM data were not used in the development of the Backman et al. (2017) Arctic-specific Aethalometer correction scheme, which could be a factor in the larger differences in absorption values at that site. Additionally, the exceptionally clean air measured at SUM means the instruments may frequently be measuring below detection limit, which could impact instrument agreement. TIK Aethalometer data are available for the entire 2012–2014 period, but the co-located MAAP absorption data only begin in summer of 2013, which is seen in Fig. 2e. Concurrent Aethalometer and MAAP absorption measurements from 2013 to 2014 at TIK agree very well ($R^2 = 0.851$). ZEP absorption datasets also generally agree on the data seasonality, though there appears to be some seasonal bias in the agreement, with the best correlation in the summer and larger differences in the corrected Aethalometer and co-located absorption data in the winter, resulting in lower overall agreement between measurement techniques ($R^2 = 0.364$).

Although agreement between Aethalometer-measured absorption and co-located instrument absorption is imperfect and variable among stations, corrected Aethalometer data from all sites are utilized in the remainder of this paper for analyses of absorption coefficients at all six Arctic monitoring stations. Using Aethalometer measurements at each location, rather than three different types of co-located reference instruments (PSAP, CLAP, and MAAP), eliminates issues with comparing data from different measurement techniques across stations. Furthermore, despite the differences in instrument agreement highlighted above, much of the difference in Aethalometer and co-located reference absorption values falls within combined instrumental uncertainties, as discussed later in this section.

Measurements from all instruments used in the analysis are reported at standard temperature and pressure (STP; $T = 0^\circ\text{C}$ and $P = 1013 \text{ hPa}$). The measurements are made at low RH (RH < 40 %) to eliminate the confounding effect of water uptake. It is not difficult to maintain a low sample RH at these sites, even for sites without heated inlets, because the

ambient dew point temperature is usually much lower than the temperature in the heated laboratories.

Quality assurance and quality control procedures were applied to the datasets at all six stations. Station scientists looked at each week of data individually to determine validity of the measurements. Additionally, there was a second stage of data review by the authors of this paper to double-check the data quality. During time periods where instruments appeared to be malfunctioning, or data were obviously influenced by local pollution (i.e., not representative of regional aerosol), data were invalidated or marked as contaminated. This helps ensure that data included here are representative of regional Arctic aerosol. At the sites in the study, measurements of absorption and scattering are made sub-hourly (data frequency: 1–5 min), though all data used in the analysis are hourly averages to improve the signal-to-noise ratio at the clean Arctic locations. All data used in this analysis are archived and accessible from the EBAS database operated by the NILU.

The variables analyzed here include extensive aerosol optical properties that depend on aerosol amount – absorption (σ_{ap}) and scattering (σ_{sp}) coefficients, and asymmetry parameter (g) – as well as intensive aerosol optical properties that are independent of the aerosol amount: single-scattering albedo (SSA) and scattering Ångström exponent (SAE). Intensive aerosol properties presented in this analysis were calculated from extensive aerosol optical property measurements.

SAE describes the wavelength dependence of the aerosol light-scattering coefficient and is inversely related to aerosol size such that large aerosols have small SAE values and vice versa (Delene and Ogren, 2002). SAE is calculated using Eq. (2):

$$\text{SAE} = -\frac{\log(\sigma_{s1}) - \log(\sigma_{s2})}{\log(\lambda_1) - \log(\lambda_2)}, \quad (2)$$

where σ_{s1} is the light-scattering coefficient at wavelength λ_1 and σ_{s2} is the light-scattering coefficient at wavelength λ_2 .

SSA is the ratio of scattering to extinction, as given in Eq. (3), and is indicative of aerosol darkness such that white aerosols (e.g., sea salt) have high SSA values and dark aerosols (e.g., black carbon) have low SSA values. SSA is calculated using Eq. (3):

$$\text{SSA} = \frac{\sigma_{\text{sp}}}{\sigma_{\text{sp}} + \sigma_{\text{ap}}}. \quad (3)$$

Aerosol asymmetry parameter, g , is a representation of the angular distribution of light scattering by an aerosol particle. The value of g can range from −1 (entirely backscattered) to 1 (entirely forward-scattered). Large particles have higher asymmetry parameters, indicating strong forward scattering. A value for g can be estimated using the backscatter fraction, b , which represents the fraction of backscattering to total scattering. Since the nephelometer measures backscattering

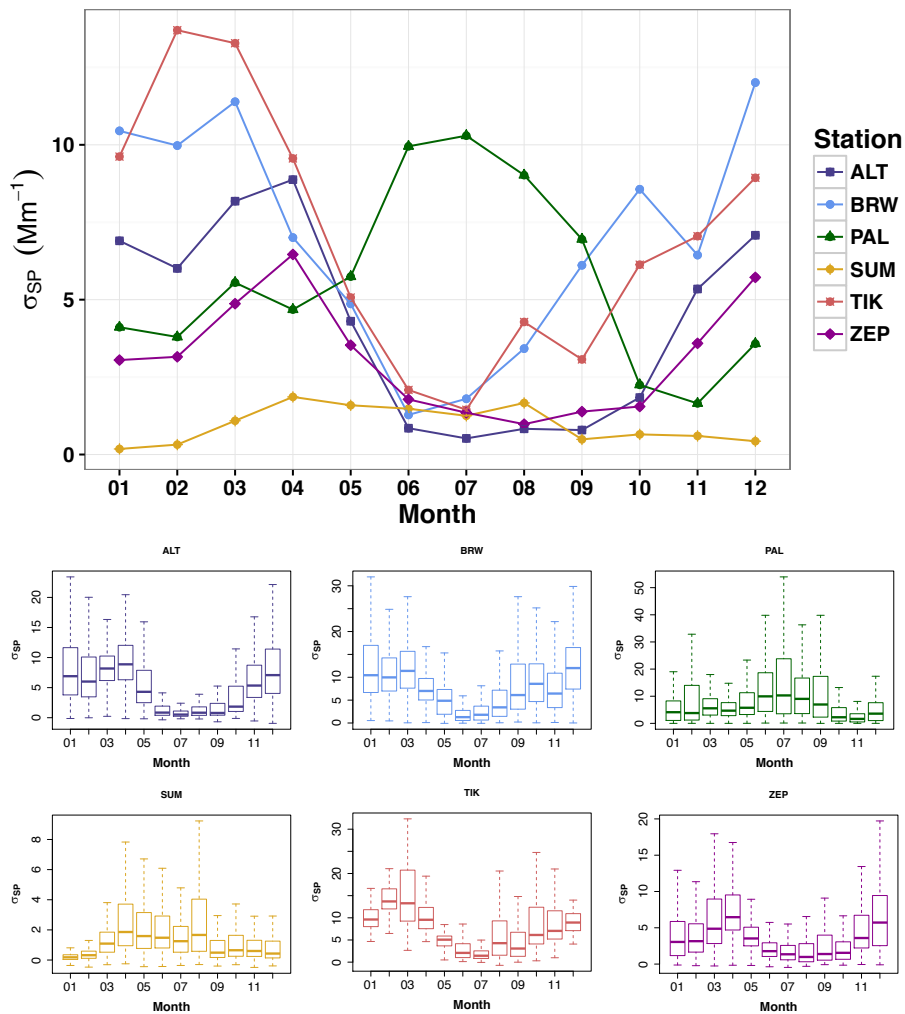


Figure 3. Seasonality of the aerosol light-scattering coefficient (σ_{sp}) at 550 nm at all sites. Large plot shows monthly medians of scattering per megameter (Mm^{-1}) at each station; subplots below show boxplots of hourly average scattering at individual sites, with horizontal line at the median, edges of the box at 25th and 75th percentiles, and whiskers at 5th and 95th percentiles. Note that y axes are different on each plot. Size cuts for the scattering measurements are as follows: 10 μm (ALT), 10 μm (BRW), 10 μm (PAL), 2.5 μm (SUM), 10 μm (TIK), and no size cut at ZEP.

and total scattering, b can be computed from nephelometer output. Here, g is computed using Eq. (4), from Andrews et al. (2006), which was derived from an empirical fit to Fig. 3 in Wiscombe and Grams (1976):

$$g = -7.143889 \cdot b^3 + 7.464439 \cdot b^2 - 3.96356 \cdot b + 0.9893. \quad (4)$$

All data were adjusted to common wavelengths (467, 525, 550, and 637 nm) for comparison among stations. For the absorption instruments with multiple wavelengths, absorption Ångström exponents were used for the wavelength adjustment. For single-wavelength absorption instruments, a $1/\lambda$ relationship (Ångström exponent = 1) was assumed for wavelength adjustments. The absorption coefficient was then

adjusted using Eq. (4):

$$\sigma_2 = \sigma_1 \cdot \left(\frac{\lambda_1}{\lambda_2} \right)^{\text{AAE}}, \quad (5)$$

where σ_1 is the measured absorption coefficient at the instrument's native wavelength λ_1 , σ_2 is the absorption coefficient adjusted to the desired wavelength λ_2 , and AAE is the absorption Ångström exponent. For those further interested, the seasonality of absorption Ångström exponent is presented in the Supplement (Fig. S2). Absorption measurements were adjusted to the same wavelength with the AAE value calculated from the 520 and 660 nm wavelength pair.

Uncertainties in PSAP- and CLAP-measured absorption coefficient measurements come from instrumental noise, unit-to-unit variability, and instrument calibration, with a total measurement uncertainty of $\sim 20\%-60\%$ (Sherman et

al., 2015; Ogren et al., 2017). Uncertainties in Aethalometer absorption coefficient measurements depend on instrumental noise, instrument calibration, and flow controller performance. The total uncertainty of the measurements depends on monitoring station, attenuation, and Aethalometer wavelength channel (Backman et al., 2017). Uncertainties in MAAP-measured absorption coefficients stem from suitability of the selected asymmetry parameter to the sampled aerosol population, uncertainty in multiple scattering of the filter, and uncertainty in diffuse fraction to yield a total uncertainty of 12 % (Petzold and Schönlinner, 2004). Uncertainties in scattering coefficient measurements stem from instrumental noise, variability in nephelometer calibration, correction to STP, correction for angular non-idealities, and correction to RH < 40 % for when samples have higher humidity (if applicable) and give a total uncertainty of 8 % (Sherman et al., 2015). More detailed information on measurement uncertainties in data from nephelometers, PSAP, and CLAP can be found in Sherman et al. (2015) and Ogren et al. (2017); details on uncertainties in Aethalometer measurements can be found in Backman et al. (2017); and uncertainties in MAAP measurements can be found in Petzold and Schönlinner (2004).

4 Results and discussion

4.1 Spatiotemporal variability of aerosol optical properties in the Arctic

The seasonality of aerosol light scattering (σ_{sp}) at the six monitoring stations reveals a diversity in magnitude and seasonality of aerosol scattering across the Arctic. Figure 3 shows monthly median values of the aerosol scattering coefficient, per megameter (Mm^{-1}), throughout the year at each station, as well as boxplots showing 5th, 25th, 50th, 75th, and 95th percentiles of hourly averaged scattering data for all months at each station. Aerosol scattering shows a strong seasonality at all sites in the study, though the seasonal cycle is not the same at each of the stations. Most sites (ALT, BRW, TIK, ZEP) show a scattering peak in the late winter and early spring, coincident with the Arctic haze phenomenon (Shaw, 1995; Quinn et al., 2007). These findings agree with many previous studies. At BRW, scattering data show a strong seasonality with values that are highest in the winter and spring during Arctic haze season, and lowest in late summer (Bodhaine, 1983, 1995; Delene and Ogren, 2002; Quinn et al., 2007). At ZEP, a study from several decades ago also finds higher scattering coefficients in the winter and lower scattering coefficients in the summer (Heintzenberg, 1982), and a study by Pandolfi et al. (2018) is also consistent with the ZEP σ_{sp} seasonal cycle presented here quite closely. The two other Arctic sites in this study exhibit distinctly different seasonal cycles. PAL measures maximum scattering coefficients in the summer and minimum scattering values in

the winter, opposite of what is observed at the first four stations. This finding agrees with previous scattering climatologies at PAL from Aaltonen et al. (2006), Aalto et al. (2002), Hatakka et al. (2003), Lihavainen et al. (2015), and Pandolfi et al. (2018). In winter the scattering values at PAL are similar to values observed at ALT, BRW, TIK, and ZEP, but in summer PAL measures notably higher scattering. PAL is located at the lowest latitude of all the sites in the study and is the closest in proximity to the European continent. Although the site itself is located on top of a fell above the tree line, the station is surrounded by a forest and thus affected by nearby biogenic emissions during the summer active vegetation season (Tunved et al., 2006; Lihavainen et al., 2009; Asmi et al., 2011). SUM is the highest in elevation of all the sites and measures free-tropospheric air much of the year. This is reflected in the substantially lower scattering measurements made at SUM compared to the other stations. The seasonal cycle of scattering at SUM also differs from the other five Arctic sites considered here, in that it has a bimodal distribution of scattering, with a peak in early spring around April and then another peak in late summer around August. There is no signature of the Arctic haze phenomenon in the Summit aerosol optical property data, which is in agreement with previous radionuclide tracer studies performed at the site (Dibb, 2007). Annual statistics – including geometric mean, median, 25th percentile, and 75th percentile – of the aerosol light-scattering coefficient are listed in Table 2 for each monitoring site.

The scattering coefficient boxplots for each station in Fig. 3 show that the spread of scattering data is generally greatest during months when the scattering coefficient values are highest at each station. In other words, at ALT, BRW, TIK, and ZEP, the winter months have the largest range of scattering values (and the largest median scattering values), while the summer months have a smaller range of scattering values (and also the lowest median scattering values). This indicates larger day-to-day aerosol variability during the Arctic haze season at these sites. PAL and SUM see a larger spread of the scattering data during summer when scattering values are the highest. Episodic long-range transport of biomass burning aerosol (i.e., smoke), long-range transport of anthropogenic aerosol from Europe, and regional biogenic emissions are likely contributing factors to the higher summer scattering values and spread of the data at these stations (Stohl et al., 2006a, 2007; Hyvärinen et al., 2011). Other contributing factors likely include long-range transport of anthropogenic aerosol from Europe as well as biogenic emissions (Hyvärinen et al., 2011; Tunved et al., 2006). In addition, at PAL, there is increased contribution from continental air masses during the summer, which contribute to the higher scattering values (Aalto et al., 2002; Asmi et al., 2011).

Figure 4 shows monthly median values of the aerosol light absorption coefficient (σ_{ap}) from corrected Aethalometer data at all six Arctic sites, as well as boxplots of absorption coefficients for all months. There is a robust annual cycle

Table 2. Statistics of aerosol optical properties at six Arctic monitoring sites, including geometric means, medians, and interquartile spread of absorption coefficient (σ_{ap}) at 550 nm, scattering coefficient (σ_{sp}) at 550 nm, single-scattering albedo (SSA) at 550 nm, and scattering Ångström exponent (SAE) at 450 and 700 nm. Percentile statistics are based on hourly averages.

Variable	Statistic	ALT	BRW	PAL	SUM	TIK	ZEP
σ_{ap} (Mm $^{-1}$)	Geometric mean	0.30	0.30	0.48	0.12	0.74	0.18
	25th percentile	0.07	0.08	0.12	0.02	0.12	0.04
	50th percentile	0.20	0.20	0.24	0.05	0.43	0.09
	75th percentile	0.41	0.39	0.49	0.11	0.98	0.23
σ_{sp} (Mm $^{-1}$)	Geometric mean	5.61	8.89	9.18	1.74	12.47	4.35
	25th percentile	1.18	3.03	1.95	0.26	2.19	1.19
	50th percentile	4.11	6.93	4.74	0.80	6.06	2.82
	75th percentile	8.31	12.05	10.97	1.93	10.88	5.53
SSA (dimensionless)	Geometric mean	0.929	0.960	0.909	0.913	0.934	0.945
	25th percentile	0.927	0.948	0.907	0.917	0.908	0.940
	50th percentile	0.949	0.969	0.956	0.954	0.950	0.963
	75th percentile	0.965	0.984	0.976	0.973	0.972	0.980
SAE (dimensionless)	Geometric mean	1.18	1.04	1.66	1.80	1.56	1.15
	25th percentile	0.85	0.58	1.22	1.41	1.30	0.64
	50th percentile	1.21	1.02	1.81	1.93	1.70	1.24
	75th percentile	1.50	1.48	2.17	2.35	2.03	1.69
g (dimensionless)	Geometric mean	0.57	0.61	0.64	0.75	0.58	0.59
	25th percentile	0.54	0.58	0.53	0.41	0.53	0.52
	50th percentile	0.60	0.63	0.60	0.61	0.59	0.57
	75th percentile	0.64	0.65	0.66	0.78	0.63	0.62

in aerosol light absorption at all of the Arctic stations. Most of the sites – including ALT, BRW, TIK, and ZEP – measure an absorption maximum in the late winter and early spring, coincident with scattering maxima and the Arctic haze season, and the lowest absorption values are measured in the summer months. This finding is in line with previous publications that find climatology of black carbon concentrations or absorption coefficients with maxima in the spring and minima in the fall (Hopper et al., 1994 (ALT); Sharma et al., 2004 (ALT); Sharma et al., 2006 (ALT); Bodhaine, 1995 (BRW); Heintzenberg, 1982 (ZEP); Eleftheriadis et al., 2009 (ZEP)). As with scattering coefficients, these stations have greatest spread in absorption data during months where absorption medians are highest. Of all the Arctic sites here, TIK has the highest absolute absorption coefficients during the winter, while PAL has the highest absorption coefficients during the summer compared to the other stations. PAL and SUM again have slightly different absorption seasonality from the rest of the sites. PAL measures maximum aerosol light absorption in the winter, with much lower values in the summer, though the summer minimum was higher than at all other stations, likely due to the closer proximity to Europe and thus potential for long-range transport. PAL notably has very large variability in absorption during the months of December, January, and February, as seen in the boxplot of absorption at PAL in Fig. 4. SUM, the most remote and highest-elevation site, shows a different cycle with its lowest absorption val-

ues in the winter and highest values in the summer, similar to the seasonality of scattering coefficients. Statistics – including geometric mean, median, 25th percentile, and 75th percentile – of the aerosol light absorption coefficient are listed in Table 2 for each monitoring site.

SSA values show seasonality at all of the Arctic sites. Figure 5 displays monthly median values of SSA, as well as boxplots of SSA for all months and all sites. ALT has relatively constant SSA values throughout most of the year, though SSA drops during July, coincident with large variability in SSA values as seen in the ALT boxplot. The SSA values at BRW are highest in the fall (September and October) and are otherwise fairly consistent the rest of the year, with the largest spread in SSA during months other than September and October. SSA values at BRW could be highest in September and October due to low sea ice extent, more open ocean, and thus the potential for more sea salt aerosol in the area (May et al., 2016). Figure 10 lends evidence for this, and it is discussed later in the paper. The multi-year annual average of SSA at BRW was found to be 0.960 (see Table 2), which agrees with the SSA averages of 0.96 presented for BRW data from 1988 to 1993 in Bodhaine (1995) and 1997 to 2000 in Delene and Ogren (2002). PAL has higher SSA values in the summer and lower SSA values in the winter. Aalto et al. (2002) find that there is an increased contribution from continental air masses in the summer at PAL. Lihavainen et al. (2015) show that SSA in summer increases

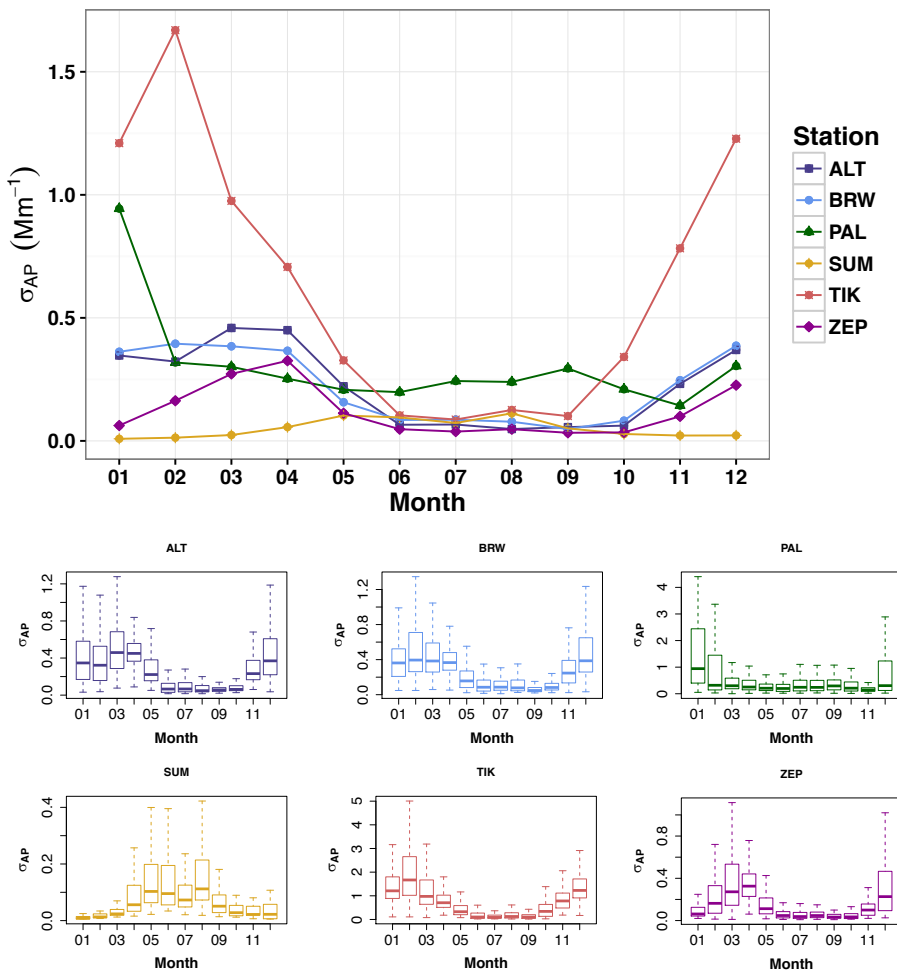


Figure 4. Seasonality of aerosol light absorption coefficient (σ_{ap}) at 550 nm at all sites. Large plot shows monthly medians of absorption per megameter (Mm^{-1}) at each station; subplots below show boxplots of hourly average absorption at individual sites, with horizontal line at the median, edges of the box at 25th and 75th percentiles, and whiskers at 5th and 95th percentiles. Note that y axes are different on each plot. Size cuts for the Aethalometer absorption measurements are as follows: 10 μm (ALT); 2.5 μm (SUM); 10 μm (TIK); and no size cut at BRW, PAL, and ZEP.

especially in continental air masses, although it is the highest throughout the year in marine air masses. The high SSA in summer is related to increasing biogenic contribution and decreasing contribution from anthropogenic sources, such as residential wood burning. SUM has similar SSA values throughout the year, except for when SSA drops to a median of 0.890 in September – quite a bit lower than the annual median SSA of 0.954. Much of the increased summer operations are winding down at SUM around September, and the related increase in flights and transportation activities at this time could contribute to the lower SSA value during September. However, no instances in the data suggest contamination spikes that need removal; rather, we speculate that the increased anthropogenic activity at SUM at this time might contribute to a darker background aerosol. TIK has the most pronounced seasonal cycle in SSA, with median values of SSA around 0.860 in the winter and higher SSA median val-

ues around 0.960 during the summer. TIK measures the darkest aerosol of all six Arctic stations during the winter. We speculate this could be due to an inversion layer trapping regional combustion aerosol produced from anthropogenic activities, energy production, and transport, mainly in the town of Tiksi and nearby villages. ZEP does not have a very distinguishable seasonality in SSA, though SSA values tend to be slightly lower during the Arctic haze season. The boxplots of SSA at ZEP indicate large variability in the SSA data at this station.

SAE for the 450 and 700 nm wavelength pair is indicative of particle size and has a seasonal signature at only some of the Arctic stations (Fig. 12). At ALT, the variability in SAE values is highest in the summer and fall months, suggesting that the site measures a variety of particle sizes during this time. However, the monthly median SAE does not show substantial change throughout the year. BRW does have sea-

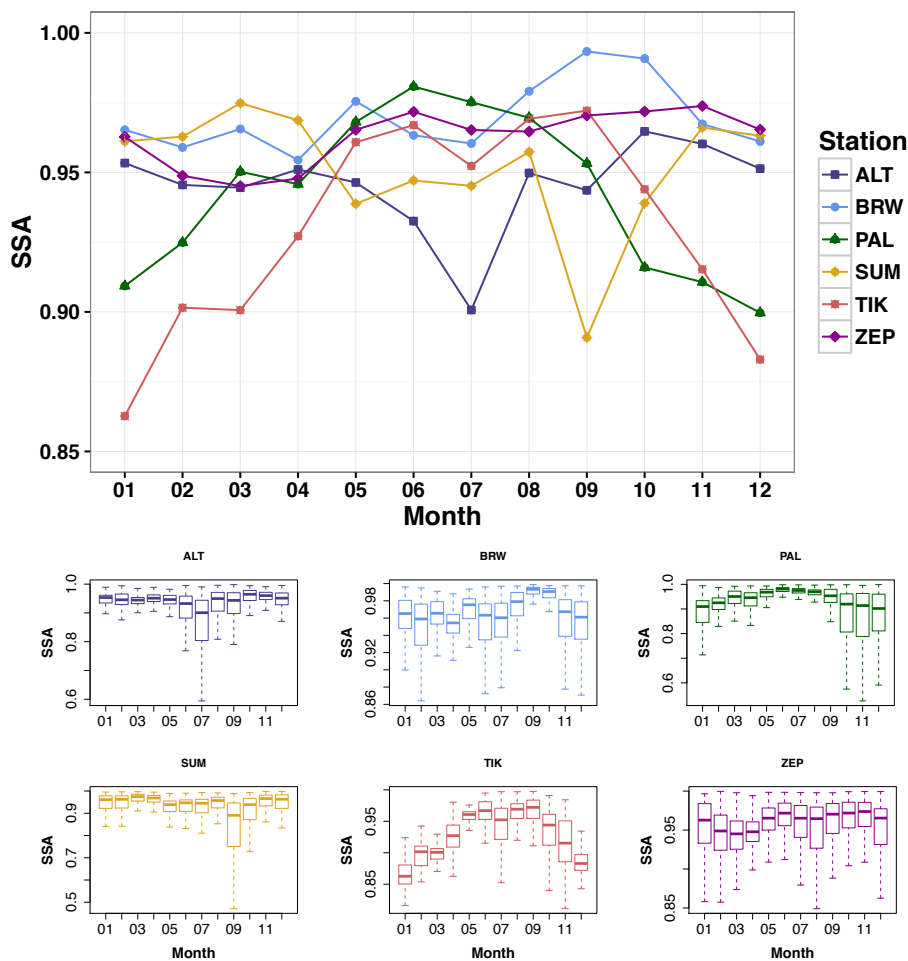


Figure 5. Seasonality of single-scattering albedo (SSA) at all sites. Large plot shows monthly medians of hourly average SSA at 550 nm at each station; subplots below show boxplots of SSA at individual sites, with horizontal line at the median, edges of the box at 25th and 75th percentiles, and whiskers at 5th and 95th percentiles. Note that y axes are different on each plot.

sonality in SAE, with lowest SAE values (larger particles) during the late summer and early fall, and higher SAE values in the spring (smaller particles). This same SAE seasonality at BRW was also observed in previous studies (Bodhaine, 1983; Delene and Ogren, 2002), and one study offers an explanation as to this seasonality with observations of an increase in sea salt when the sea ice melts in summer months (Quinn et al., 2002). PAL has a different seasonality, with highest SAE values in the summer and lowest SAE values in the winter and early spring, which agrees with findings from Aaltonen et al. (2006) and Lihavainen et al. (2015). The statistics of SAE in Table 2 show an average SAE of 1.66 at PAL, which is close to the average of 1.7 ± 0.7 that is reported in Lihavainen et al. (2015) and the median of 1.8 reported by Pandolfi et al. (2018). SUM statistical values of SAE are not directly comparable to the other Arctic sites due to its $2.5\text{ }\mu\text{m}$ size cut inlet, which limits measurements of large particles that would yield smaller SAE values. There is very little variability in SAE at SUM throughout the year, as the boxplot

shows that medians of SAE in all months fall within the interquartile spread of SAE in all other months. However, it is notable that SUM generally has some of the highest SAE values of all six Arctic sites, meaning it is measuring some of the smallest aerosol of these Arctic stations. These high SAE values are likely due to the remote, high-elevation location of SUM, which means larger particles fall out or are removed before reaching the monitoring station. Additionally, the long distance to the ocean from SUM means there is likely no sea salt measured, which can be a likely source for coarse aerosols in the Arctic. TIK has higher SAE values in March and October, with lower SAE values the rest of the year. Additionally, TIK sees the largest variability in SAE between the months of June and September. This large variability could be attributed to Siberian wildfire events that occur sporadically during the summer or to the secondary particle formation and growth by biogenic precursors that affect the site sporadically during the summer season (Asmi et al., 2016). Finally, ZEP measures smaller aerosols (larger

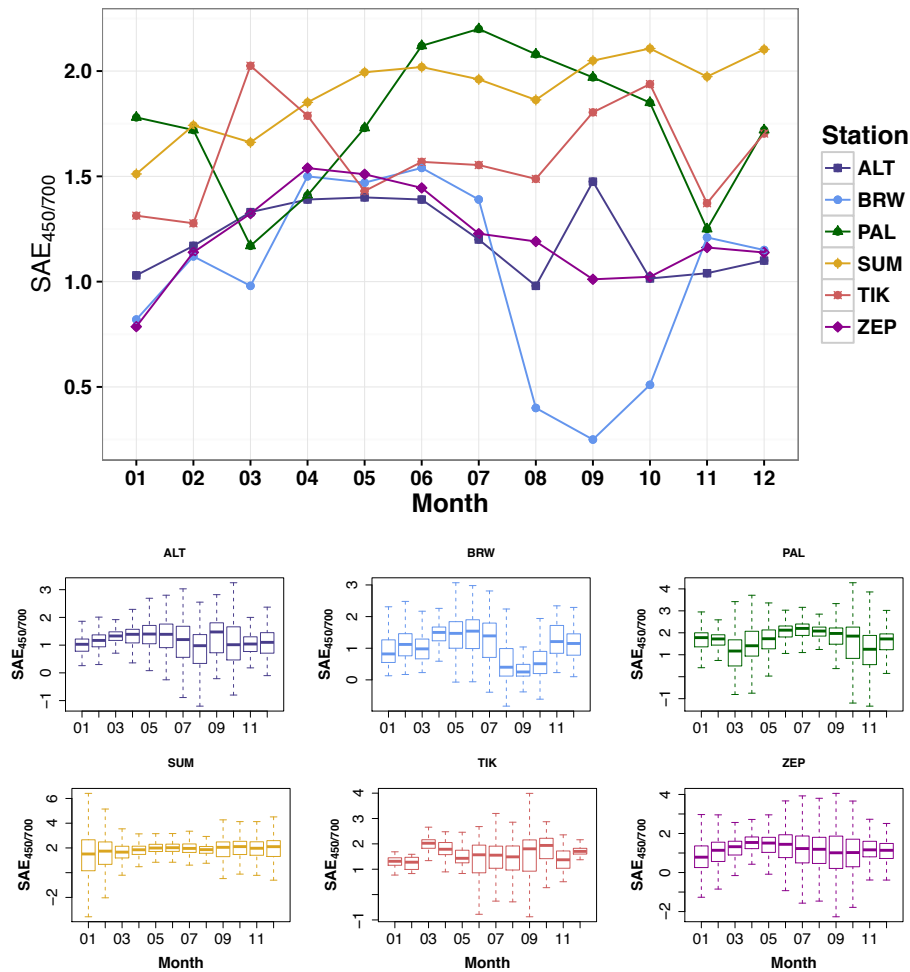


Figure 6. Seasonality of scattering Ångström exponent (SAE) at all sites. Large plot shows monthly medians of hourly average SAE at the 450 and 700 nm wavelength pair at each station; subplots below show boxplots of SAE at individual sites, with horizontal line at the median, edges of the box at 25th and 75th percentiles, and whiskers at 5th and 95th percentiles. Note that y axes are different on each plot.

SAE values) in the spring and larger aerosols in the late summer, in accordance with the Arctic haze phenomenon and in agreement with seasonal cycle of SAE at ZEP presented in Pandolfi et al. (2018). Mean SAE at ZEP (see Table 2) is 1.15, which is slightly higher than the SAE median of just less than 1 presented in Pandolfi et al. (2018), which used ZEP data from 2010 to 2014.

The variability of the asymmetry parameter, g , is similar for all sites except for SUM. Figure 7 shows that ALT, BRW, PAL, TIK, and ZEP have highest values of g in the winter and lowest values in the summer. It is clear in these station subplots of Fig. 7 that the variability in g is largest during the summer months. This could be due to higher noise in the nephelometer when scattering measurements are really low. In contrast, SUM shows the opposite seasonal cycle in asymmetry parameter, with g highest in the late summer and lowest in the late winter. PAL and ZEP g seasonalities are in agreement with those presented in Pandolfi et al. (2018).

To our knowledge, asymmetry parameter values for the other four sites have not been previously presented in the literature. However, Delene and Ogren (2002) did present the seasonality of backscatter fraction (b) for BRW; because g is expected to vary inversely with b , and because they find that b is highest in the summer and lowest in the winter, their results are also consistent with those reported here. Andrews et al. (2011) and Pandolfi et al. (2018) report a general tendency for g to increase as σ_{sp} increases for mountain sites and European ACTRIS sites, respectively. The same tendency was found for the Arctic sites here (not shown). The lower g values at the five Arctic sites during the summer indicate the presence of smaller particles, probably due in part to wet scavenging of larger particles and/or new particle formation. Both processes tend to be more common in the summer (e.g., Freud et al., 2017) and are consistent with the lower scattering coefficients observed in the summer. Higher g values throughout the rest of the year represent larger particles,

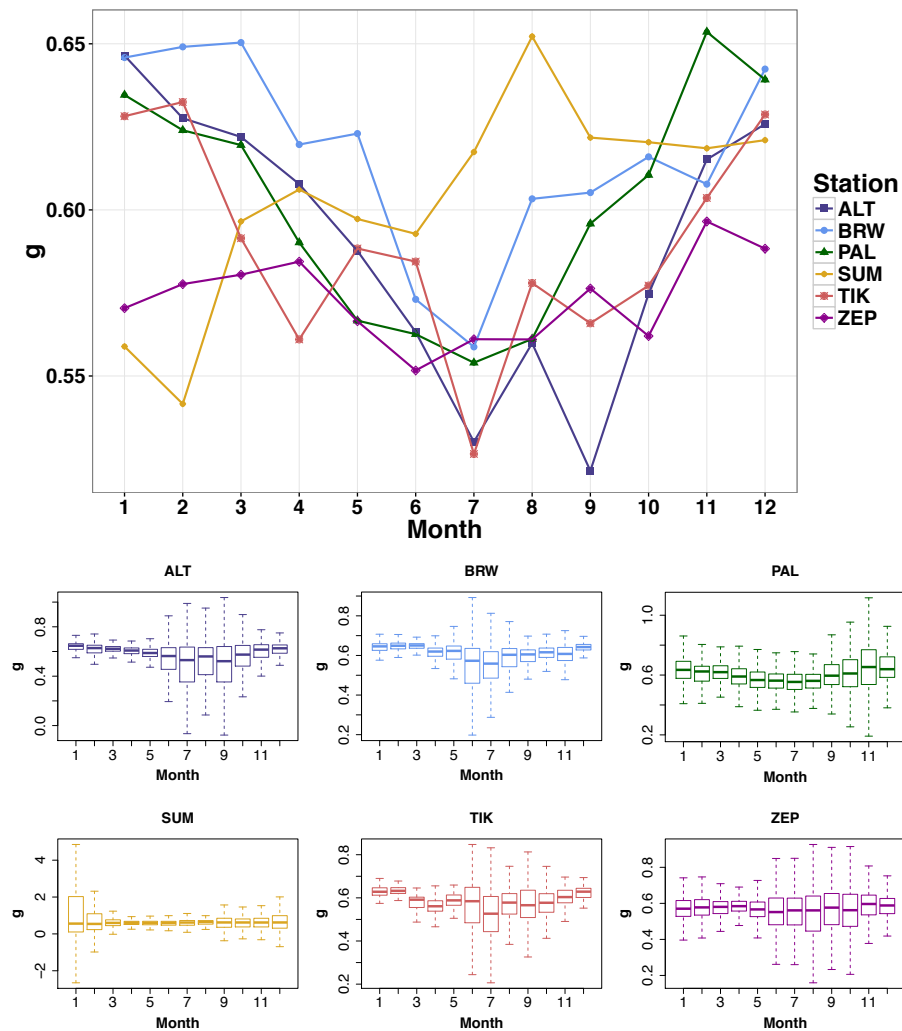


Figure 7. Seasonality of aerosol asymmetry parameter (g) at all sites. Large plot shows monthly medians of hourly average g at 550 nm at each station; subplots below show boxplots of g at individual sites, with horizontal line at the median, edges of the box at 25th and 75th percentiles, and whiskers at 5th and 95th percentiles. Note that y axes are difference on each plot.

perhaps due to long-range transport. BRW, for example, has been impacted by Asian dust in the spring (e.g., Stone et al., 2007). However, SAE seasonality does not support this pattern at every site (the inconsistent relationship between SAE and g is also discussed in detail in Pandolfi et al., 2018). This indicates that the specific shape of the aerosol size distribution at each site will have a role in determining g and SAE at Arctic sites as different aerosol parameters are sensitive to different parts of the size distribution (e.g., Collaud Coen et al., 2007).

4.2 Systematic variability of aerosol optical properties in the Arctic

The systematic variability of aerosol optical properties refers to how aerosol parameters covary with each other. Analysis of the systematic relationships between aerosol optical

properties is useful because it can provide insight to aerosol sources and atmospheric processes (Andrews et al., 2011; Toledoano et al., 2007) and can also be a good metric for comparing consistency between aerosol models and measurements.

The systematic variability plots shown here were created by binning the hourly averages of aerosol light-scattering coefficient values into 2 Mm^{-1} bins between 0 and 20 Mm^{-1} (this scattering range captures most of the station data (Fig. 3); a scattering coefficient of 20 Mm^{-1} corresponds to the following percentiles at each station: 97.7 at ALT, 91.2 at BRW, 87.9 at PAL, 99.5 at SUM, 92.1 at TIK, and 98.2 at ZEP) and then calculating and plotting median values of the absorption coefficient, SAE, and SSA for each bin. This was repeated for 0.02 bins of SSA and plotting median values for SAE. As in Andrews et al. (2011), only bins that had a standard error (standard error is the standard deviation of the

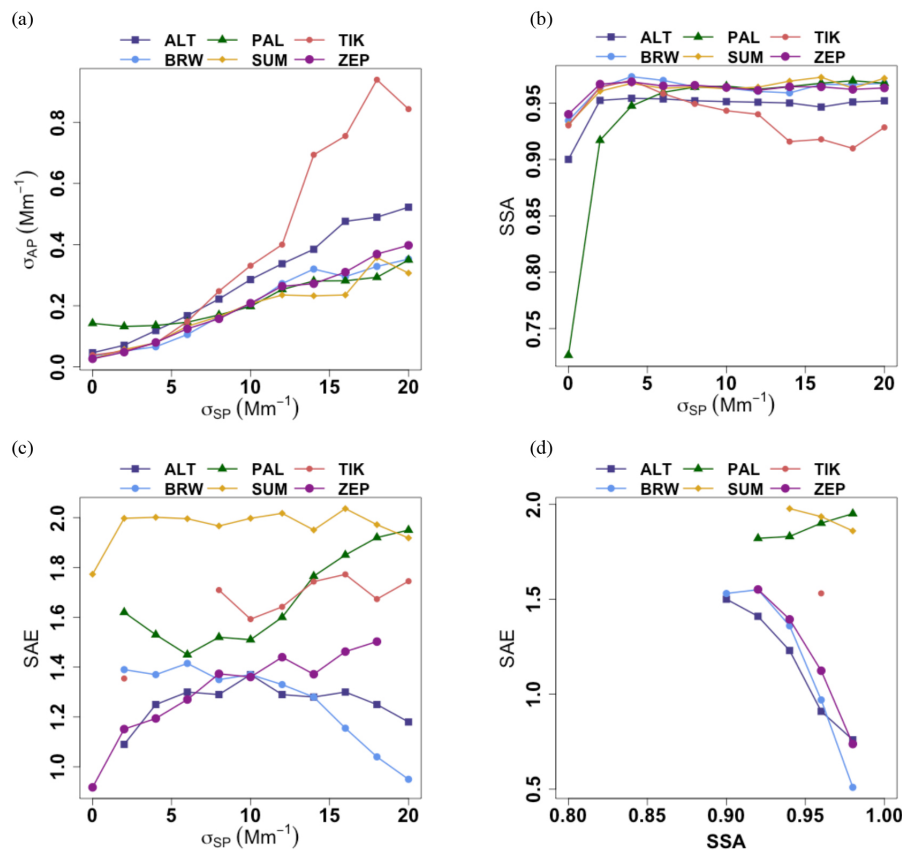


Figure 8. Systematic variability of median aerosol optical properties: (a) absorption varying with scattering coefficient, (b) single-scattering albedo varying with scattering coefficient, (c) scattering Ångström exponent varying with scattering coefficient, and (d) scattering Ångström exponent varying with single-scattering albedo.

sample divided by the square root of the number of points in the sample) less than 2 % of the typical value of that variable were included, with 2 % of the typical values considered to be ~ 0.02 for SSA, ~ 0.04 for SAE, and $\sim 0.1 Mm^{-1}$ for absorption coefficient. Bins with a larger standard error were omitted, since they may not be representative of actual aerosol systematic variability at the site.

The absorption coefficient varies with the scattering coefficient almost linearly, such that absorption increases as scattering increases as shown in Fig. 8a. One interpretation of this linear relationship between these scattering and absorption coefficients is that the scattering and absorbing aerosols are coming from the same sources and are subject to similar removal processes during transport to the site. This is consistent with systematic variability analysis from Andrews et al. (2011) that looked at data from mountain sites. Delene and Ogren (2002) also show this systematic variability for BRW, over the same scattering range ($0\text{--}20 Mm^{-1}$) shown here, though Delene and Ogren (2002) find that absorption at BRW decreases at scattering values above $\sim 20 Mm^{-1}$. Higher scattering values were not investigated here. Up to a scattering coefficient of about $8 Mm^{-1}$, most of the sta-

tions (except for PAL) have a very similar ratio of absorption to scattering, especially at lower absorption and scattering coefficients. This could be representative of a background Arctic aerosol being measured at all stations during relatively clean conditions. Where the ratios differ between stations at higher scattering and absorption values, a variety of local or long-range transport sources could be influencing each station differently and changing this ratio. PAL looks different than other stations at the low loadings, where there is a higher ratio of absorption to scattering. Above a scattering coefficient of $8 Mm^{-1}$, ALT and TIK show a different systematic variability than the other stations, where ALT has a higher absorption-to-scattering ratio, and TIK has a much higher absorption-to-scattering ratio at high aerosol loadings. This suggests that at TIK high-aerosol-concentration events are strongly influenced by absorbing aerosols, which is consistent with the finding of Asmi et al. (2016).

Single-scattering albedo varies with scattering such that the lowest scattering coefficient bins are accompanied by relatively low SSA values, and SSA values plateau with higher scattering values – see Fig. 8b. This finding follows the same pattern but with a much weaker dependence than what was

found for mountain sites in Andrews et al. (2011) and shows a much weaker relationship than what was found for continental North American sites in Sherman et al. (2015). It should be noted that comparisons with systematic variability relationships for other site types are difficult since this Arctic analysis only looks at scattering from 0 to 20 Mm^{-1} , while the aforementioned papers analyze a much greater range of scattering coefficients. The SSA–scattering relationship here suggests that whiter aerosols are preferentially scavenged such that darker aerosols remain at the lowest aerosol loadings (lowest scattering coefficients). Delene and Ogren (2002) find that SSA at BRW decreases slightly between scattering coefficient bins between 0 and 10 Mm^{-1} but that SSA increases after that as scattering increases. TIK looks different from the other Arctic sites since SSA increases with scattering only up until a scattering coefficient of $\sim 5 \text{ Mm}^{-1}$, after which SSA decreases. This means higher aerosol loadings at TIK have darker aerosol, which could be representative of fresh smoke emissions affecting the site at high aerosol loadings, in accordance with the systematic variability of absorption with scattering.

The scattering Ångström exponent varies with scattering in diverse ways at the six Arctic stations, as indicated in Fig. 8c. At sites like ALT, SUM, and TIK, SAE does not vary much with changes in scattering. BRW generally shows decreases in SAE (or increases in particle size) as scattering increases. Delene and Ogren (2002) show that the aerosol particles at BRW tend to be largest (lowest SAE) and whitest (highest SSA) during the summer (lowest scattering values), which they attribute to the contribution of marine aerosol when the sea ice melts. Chemical analysis has supported this conclusion (Quinn et al., 2002), though the systematic variability plots shown here do not provide the means to analyze this seasonality. ZEP shows distinctly different systematic variability from BRW, in that SAE increases (decreasing particle size) as scattering increases. The asymmetry parameter provides another means of investigating changes in particle size distribution with loading, and the plot of scattering vs. asymmetry parameter and the associated discussion are included in the Supplement.

Figure 8d shows that SAE also varies with SSA. At ALT, BRW, and ZEP, SAE decreases as SSA increases. This indicates that the more scattering particles are typically larger at these sites (e.g., sea salt), and more absorbing particles are typically smaller (e.g., black carbon). There are not enough data that meet the standard error threshold to detect systematic variability in these properties at TIK. PAL and SUM do not show substantial systematic variability in these optical parameters, likely due to the $2.5 \mu\text{m}$ size cut inlet (SUM) and/or remote, high-elevation location (SUM) that limits the measurement of larger particles and thus yields consistently high SAE values. The different behavior at PAL is likely due to the location of the site (lowest latitude) and difference in the vegetation surrounding the station as discussed earlier.

4.3 Back-trajectory analysis

Back-trajectory analyses are widely used to investigate the effect of air mass pathway on atmospheric constituents measured at a particular place (Fleming et al., 2012). The trajectory method involves calculating air parcel movement from the monitoring site back in time to yield the back trajectory of the parcel (Draxler and Hess, 1998). Here, individual 7-day back trajectories computed for each of the six Arctic sites are overlaid and colored by frequency of back-trajectory occurrence in each grid box to create a density plot of air mass history for each station.

In this work, the air mass back-trajectory analysis was conducted using the NOAA Hybrid Single-Particle Lagrangian Integrated Trajectory model (HYSPLIT) version 4.9 (Draxler and Hess, 1998; Stein et al., 2015). The HYSPLIT model was run for 7-day back trajectories, using an ensemble method. The ensemble method offsets the meteorological grid by one grid point in the horizontal and 1 % of the surface pressure in the vertical, which produces 27 back trajectories for possible offsets in the horizontal and vertical, thus accounting for uncertainties in the gridded meteorological data. The meteorological data used for the trajectories were from the NCEP/GDAS dataset with a 1° horizontal resolution and 23 pressure levels (Kanamitsu, 1989).

Figure 9 shows density plots of each 7-day back-trajectory path computed at each station over the period of interest (2012–2014), colored by frequency at which the air mass passed through the given grid cell. Regions colored in red represent regions through which air masses most frequently traveled en route to the monitoring station, and regions colored in blue represent areas through which an air mass passed least frequently en route to the monitoring station. All trajectory altitudes are included in plots in Fig. 9.

For all measurement sites, air masses arriving at the site obviously pass most frequently through regions closest to the stations. The differences between summer and winter back trajectories at each site are subtle and do not reflect the large seasonality observed in aerosol optical property measurements throughout the Arctic. This is consistent with similar back-trajectory frequency analyses at ALT (Sharma et al., 2006; Huang et al., 2010). This could be because the wide range of synoptic-scale weather patterns averaged into 3 years of back-trajectory data obscure seasonality in large-scale air mass paths. One feature that is evident from Fig. 9 is that SUM does not seem to have the same air mass origin as the other sites. Even the closest station, ALT, does not overlap much with calculated source areas for SUM. This feature is even clearer when only trajectory altitudes below 500 m a.g.l. are considered. This supports the earlier argument that, due to the altitude and location of SUM on top of the Greenland ice shelf, the aerosol arriving at the stations is very different compared to the other sites that are almost exclusively coastal. The strong seasonality observed in the aerosol optical properties at each of the Arctic sites is

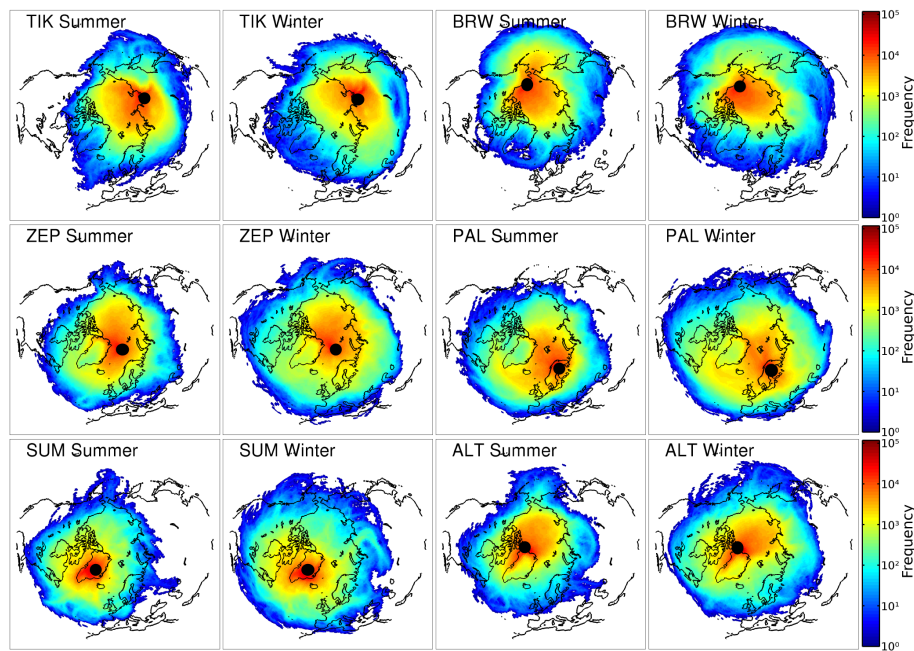


Figure 9. Seven-day back trajectories at each of the six Arctic stations, separated by summer (May–October) and winter (November–April) months. Colors represent frequency (units of hours per 2 years) at which an air parcel travels over that region before arriving at the station, in other words, residence time of air in that location. These plots show data from all trajectory altitudes. Black dots show station location.

likely not due to large changes in air mass back trajectories from season to season. If the seasonality of the aerosol parameters is not described by differences in air mass origin, then we speculate that the aerosol sources (both natural and anthropogenic) differ in type and magnitude from season to season and may explain the temporal variability of aerosols in the Arctic. This notion is supported by previous studies (Eleftheriadis et al., 2009; Asmi et al., 2016; Wang et al., 2014; Sharma et al., 2013). Alternatively, it is possible that much longer back trajectories would elucidate additional information on seasonal differences in air mass origin for long-distance aerosol transport to the Arctic (Qi et al., 2017). For example, work by Hirdman et al. (2010) uses 20-day back trajectories from FLEXPART and suggests stronger seasonal differences in aerosol transport pathways than were found here. Using much longer back-trajectory calculations in this study would, however, also be associated with much greater uncertainties in the spatial domain, which is why the trajectory calculations were restricted to 7 days.

For further exploration of why aerosol sources (rather than transport) might differ in type and magnitude from season to season, Fig. 10 affords insight into how the land type over which an air mass travels might affect the aerosols within it. Figure 10 shows the percent of air mass residence time spent above different land types before arriving at each monitoring station for each month of the year. The data used for sea ice extent came from the National Snow and Ice Data Center's Sea Ice Index dataset (Fetterer et al., 2015). The green bars represent land (with no distinction between snow-

covered and bare land areas), light blue bars represent sea ice, and dark blue bars represent open water. There is a clear seasonality in land type over which air masses travel before arriving at each measurement site. At all sites except SUM, air masses travel more over open water during the summer when sea ice has melted. This provides a source for sea salt and other marine aerosol during the summer that is much less likely at other times in the year. The result that the same source region overlaps with open ocean in summer and sea ice in winter, and thus yields different aerosol, is supported by similar findings from Shaw et al. (2010). TIK, PAL, and SUM are similar in that most of the air mass residence time is spent above land at all times of the year, but especially so in winter. ALT, ZEP, and BRW are similar in that the air masses arriving at these stations spent more time, compared to the other sites, over sea ice and much less time over land. This could explain why ALT, ZEP, and BRW have very similar seasonality of aerosol light-scattering and absorption coefficients, while TIK, PAL, and SUM have different seasonality that may be indicative of varying land-based aerosol sources. More work is needed, using chemical analyses or footprint analyses, to better understand how air mass transport contributes to the different aerosol seasonality at each of the six Arctic sites.

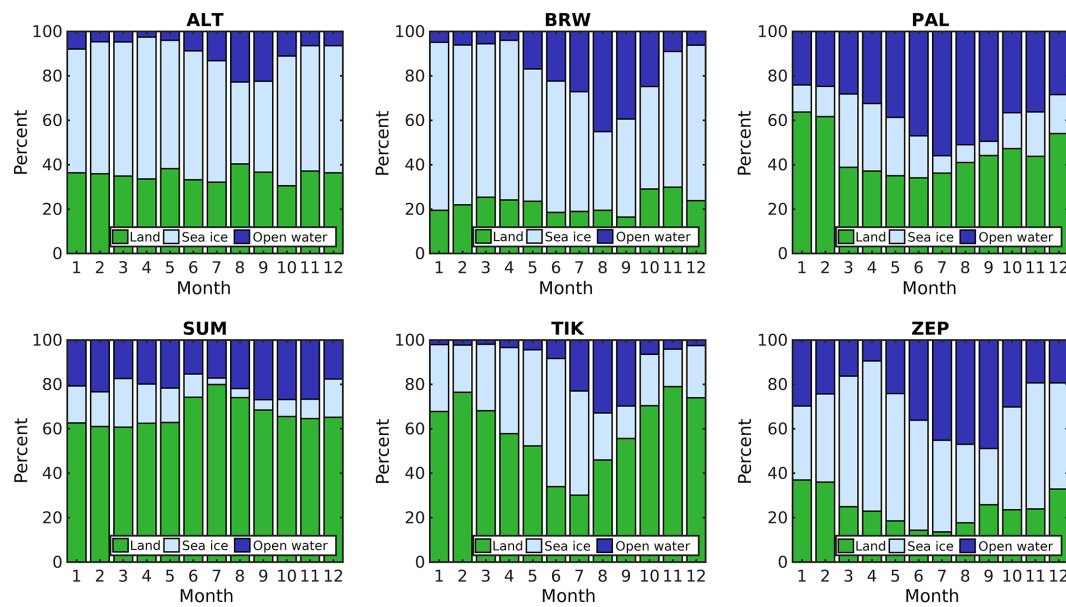


Figure 10. Percent of air mass residence time during the past 7 days spent above different land types before arriving at monitoring station for each month of the year. Green represents land (with no distinction between snow-covered and bare land areas), light blue represents sea ice, and dark blue represents open water.

5 Conclusions

Seasonal cycles of aerosol optical properties from six Arctic monitoring stations have been presented here. Aerosol optical properties were derived from common absorption and scattering instruments (Aethalometers and nephelometers, respectively) at the stations, were evaluated and corrected under common quality control procedures, and were presented at standard temperature and pressure and low relative humidity to ensure high quality and comparability of data across stations.

The extensive aerosol optical properties, dependent on amount of aerosol, showed strong seasonality at all of the Arctic sites analyzed here. The magnitude and variability of the aerosol light-scattering coefficient vary substantially among stations, with SUM measuring the lowest annual mean scattering coefficients (1.74 Mm^{-1}) and TIK measuring the highest annual mean scattering coefficients (12.47 Mm^{-1}). ALT, BRW, TIK, and ZEP have maximum scattering values in the spring, and lowest in the summer, while PAL and SUM have lowest scattering values in the winter and highest in the summer. The magnitude and variability of the aerosol light absorption coefficient are slightly less variable between stations compared to scattering. The lowest annual mean absorption coefficient is measured at SUM (0.12 Mm^{-1}), while the highest annual mean absorption coefficient is measured at PAL (0.48 Mm^{-1}). Stations ALT, BRW, PAL, TIK, and ZEP all have a seasonal cycle that reflects high absorption in the winter and spring, and low absorption in the summer, though the exact timing of the ab-

sorption maxima and minima differs among stations. SUM absorption is unique from the other sites in that the highest absorption values are in summer, and lowest absorption values are in winter. The distinctiveness of the SUM seasonality is likely due to its remote and high-elevation location.

The intensive aerosol optical properties, which are independent of aerosol amount, also show strong seasonality at all six Arctic stations. Furthermore, quite high SSA values at all stations are evident in our data. The range of annual mean single-scattering albedo values at the sites is from 0.909 at PAL to 0.960 at BRW. The annual mean scattering Ångström exponent values range from 1.04 at BRW to 1.80 at SUM. The annual mean aerosol asymmetry parameter values range from 0.57 at ALT to 0.75 at SUM. The seasonalities of these variables suggest that aerosol source and removal mechanisms are likely different from month to month at a given site and from site to site throughout the Arctic.

Systematic variabilities of the aerosol optical parameters measured in the Arctic provide insight into atmospheric processes near the monitoring stations. Generally, absorption coefficients increase as scattering coefficients increase at all of the sites. However, the ratio of absorption to scattering is different across sites and aerosol loadings, with TIK and ALT showing higher absorption-to-scattering ratios at high aerosol loadings, and PAL showing higher absorption-to-scattering ratios at low aerosol loadings compared to the other stations. Single-scattering albedo is low at low loadings for all of the six Arctic sites, and SSA increases with increasing scattering for most sites. TIK is an exception to this observation, since darker aerosol (low SSA) is mea-

sured at higher scattering coefficients, which suggests absorbing aerosol (e.g., black carbon) may be associated with high-aerosol-loading events (e.g., anthropogenic emissions, Siberian wildfires). Our findings of generally higher aerosol absorption and lower SSA for both TIK and PAL during winter could suggest a closer proximity to anthropogenic activities, which is supported by their geographic locations since they are both continental Eurasian locations – closer to forest fires, long-range transport, and regional emissions.

Back-trajectory analysis showed little evidence of seasonality in air mass origin between winter and summer months. The analysis further strengthens the observation that SUM is different from the other stations because other stations seem to receive little air from the same areas that SUM does. Data on sea ice combined with air mass movement indicated that TIK and PAL receive the most continental air masses, whereas BRW, PAL, and ZEP are the stations with the potential to be most influenced by marine aerosol.

A persistent and important theme in the findings of this paper is that aerosol optical properties vary widely with season at any individual site, and they vary widely from station to station throughout the Arctic. This result is important, since it means that the Arctic cannot be treated as a uniform region, spatially or temporally, in climate models or in remote-sensing retrieval algorithms. Rather, the wide spatiotemporal variability of aerosol in the Arctic needs to be considered in order to properly represent the climate of this sensitive region.

Data availability. Data used in this article are archived and accessible from the EBAS database operated at the Norwegian Institute for Air Research (NILU) (<http://ebas.nilu.no>). The aethalometer dataset used in this article can be found at <https://doi.org/10.21336/gen.1> (Backmann, 2018).

Supplement. The supplement related to this article is available online at: <https://doi.org/10.5194/acp-18-11599-2018-supplement>.

Author contributions. LS created the dataset, completed data analysis, created Figs. 1–8, and wrote most of the manuscript. JB corrected the Aethalometer data, contributed the trajectory analysis and Figs. 9 and 10, and wrote most of the trajectory analysis section. EA helped write the introduction section and helped guide the data analysis. JO and EA helped guide the data analysis and interpret results. SS and TU provided organizational support and helped guide data analysis. TU, SS, KE, SV, MB, PT, and AJ all provided station data and provided input for interpretation of results at the individual stations.

Competing interests. The authors declare that they have no conflict of interest.

Acknowledgements. Thank you to all of the station technicians at these Arctic monitoring sites who work in difficult Arctic conditions to help acquire the data presented here. The authors would like to acknowledge the International Arctic System for Observing the Atmosphere (IASOA) aerosol working group for coordination of the project and contribution of expertise to this analysis. Data management is provided by the WMO Global Atmosphere Watch World Data Centre for Aerosol. This project has received funding from the European Union's Horizon 2020 research and innovation program under grant agreement no. 654109 (ACTRIS). The Finnish Meteorological Institute acknowledges the Academy of Finland project “Greenhouse gas, aerosol and albedo variations in the changing Arctic” (project number 269095); the Novel Assessment of Black Carbon in the Eurasian Arctic: From Historical Concentrations and Sources to Future Climate Impacts (NABCEA) (project number 296302); the Academy of Finland Centre of Excellence program (project number 307331); and EU H2020 project INTAROS (project ID: 727890) for financial support. Funding from the NOAA Climate Program Office provided partial support for data analysis and measurements at Barrow and Summit. The authors would like to thank the staff of the Canadian Forces Service for maintenance of the Alert station. The light-scattering measurements at Alert were initiated by Richard Leaitch.

Edited by: Nikos Hatzianastassiou

Reviewed by: three anonymous referees

References

- Aalto, B. T., Hatakka, J., Paatero, J., Tuovinen, J., Aurela, M., Laurila, T., Holmen, K., Trivett, N., and Viisanen, Y.: Tropospheric carbon dioxide concentrations at a northern boreal site in Finland: Basic variations and source areas, *Tellus*, 54B, 110–126, <https://doi.org/10.1034/j.1600-0889.2002.00297.x>, 2002.
- Aaltonen, V., Lihavainen, H., Kerminen, V.-M., Komppula, M., Hatakka, J., Eneroth, K., Kulmala, M., and Viisanen, Y.: Measurements of optical properties of atmospheric aerosols in Northern Finland, *Atmos. Chem. Phys.*, 6, 1155–1164, <https://doi.org/10.5194/acp-6-1155-2006>, 2006.
- Aliabadi, A. A., Staebler, R. M., and Sharma, S.: Air quality monitoring in communities of the Canadian Arctic during the high shipping season with a focus on local and marine pollution, *Atmos. Chem. Phys.*, 15, 2651–2673, <https://doi.org/10.5194/acp-15-2651-2015>, 2015.
- Anderson, T. L. and Ogren, J. A.: Determining aerosol radiative properties using the TSI 3563 integrating nephelometer, *Aerosol Sci. Tech.*, 29, 57–69, <https://doi.org/10.1080/02786829808965551>, 1998.
- Andrews, E., Sheridan, P. J., Fiebig, M., McComiskey, A., Ogren, J. A., Arnott, P., Covert, D., Elleman, R., Gasparini, R., Collins, D., Jonsson, H., Schmid, B., and Wang, J.: Comparison of methods for deriving aerosol asymmetry parameter, *J. Geophys. Res.*, 111, D05S04, <https://doi.org/10.1029/2004JD005734>, 2006.
- Andrews, E., Ogren, J. A., Bonasoni, P., Marinoni, A., Cuevas, E., Rodriguez, S., Sun, J. Y., Jaffe, D. A., Fischer E. V., Baltensperger, U., Weingartner, E., Collaud Coen, M., Sharma, S., Macdonald, A. M., Leaitch, W. R., Lin, N.-H., Laj, P., Arsov, T.,

- Kalapov, I., and Sheridan, P.: Climatology of aerosol radiative properties in the free troposphere, *Atmos. Res.*, 102, 365–393, <https://doi.org/10.1016/j.atmosres.2011.08.017>, 2011.
- Anisimov, I. A., Vaughan, D. G., Callaghan, T. V., Furgal, C., Marchant, H., Prowse, T. D., Vilhjálmsson, H., and Walsh, J. E.: Polar regions (Arctic and Antarctic), Climate Change 2007: Impacts, Adaptation and Vulnerability. Contribution of Working Group II to the Fourth Assessment Report of the Intergovernmental Panel on Climate Change, edited by: Parry, M. L., Canziani, O. F., Palutikof, J. P., can der Linden, P. J., and Hanson, C. E., Cambridge University Press, Cambridge, 653–685, 2007.
- Asmi, E., Kivekäs, N., Kerminen, V.-M., Komppula, M., Hyvärinen, A.-P., Hatakka, J., Viisanen, Y., and Lihavainen, H.: Secondary new particle formation in Northern Finland Pallas site between the years 2000 and 2010, *Atmos. Chem. Phys.*, 11, 12959–12972, <https://doi.org/10.5194/acp-11-12959-2011>, 2011.
- Asmi, E., Kondratyev, V., Brus, D., Laurila, T., Lihavainen, H., Backman, J., Vakkari, V., Aurela, M., Hatakka, J., Viisanen, Y., Uttal, T., Ivakhov, V., and Makshtas, A.: Aerosol size distribution seasonal characteristics measured in Tiksi, Russian Arctic, *Atmos. Chem. Phys.*, 16, 1271–1287, <https://doi.org/10.5194/acp-16-1271-2016>, 2016.
- Backman, J., Schmeisser, L., Virkkula, A., Ogren, J. A., Asmi, E., Starkweather, S., Sharma, S., Eleftheriadis, K., Uttal, T., Jefferson, A., Bergin, M., Makshtas, A., Tunved, P., and Fiebig, M.: On Aethalometer measurement uncertainties and an instrument correction factor for the Arctic, *Atmos. Meas. Tech.*, 10, 5039–5062, <https://doi.org/10.5194/amt-10-5039-2017>, 2017.
- Backman, J., Schmeisser, L., Virkkula, A., Ogren, J. A., Asmi, E., Starkweather, S., Sharma, S., Eleftheriadis, K., Vratolis, S., Uttal, T., Tunved, P., Jefferson, A., Bergin, M., Makshtas, A., and Fiebig, M.: Time series of aerosol light-absorption coefficients from Aethalometers at six Arctic stations between 2012 and 2014, available at: <https://doi.org/10.21336/gen.1>, last access: 15 August 2018.
- Bintanja, R. and Selten, F. M.: Future increases in Arctic precipitation linked to local evaporation and sea-ice retreat, *Nature*, 509, 479–482, <https://doi.org/10.1038/nature13259>, 2014.
- Bodhaine, B. A.: Aerosol measurements at four background sites, *J. Geophys. Res.*, 88, 10753–10768, <https://doi.org/10.1029/JC088iC15p10753>, 1983.
- Bodhaine, B. A.: Aerosol absorption measurements at Barrow, Mauna Loa and the South Pole, *J. Geophys. Res.*, 100, 8967–8975, <https://doi.org/10.1029/95JD00513>, 1995.
- Bond, T. C., Anderson, T. L., and Campbell, D.: Calibration and intercomparison of filter-based measurements of visible light absorption by aerosols, *Aerosol Sci. Tech.*, 30, 582–600, <https://doi.org/10.1080/027868299304435>, 1999.
- Chapin, F. S., Sturm, M., Serreze, M. C., McFadden, J. P., Key, J. R., Lloyd, A. H., McGuire, A. D., Rupp, T. S., Lynch, A. H., Schimel, J. P., Beringer, J., Chapman, W. L., Epstein, H. E., Euskirchen, E. S., Hinzman, L. D., Jia, G., Ping, C.-L., Tape, K. D., Thompson, C. D. C., Walker, D. A., and Welker, J. M.: Role of land-surface changes in arctic summer warming, *Science*, 310, 657–660, <https://doi.org/10.1126/science.1117368>, 2005.
- Collaud Coen, M., Weingartner, E., Nyeki, S., Cozic, J., Henning, S., Verheggen, B., Gehrig, R., and Baltensperger, U.: Long-term trend analysis of aerosol variables at the high-alpine site Jungfraujoch, *J. Geophys. Res.*, 112, D13213, <https://doi.org/10.1029/2006JD007995>, 2007.
- Collaud Coen, M., Weingartner, E., Apituley, A., Ceburnis, D., Fierz-Schmidhauser, R., Flentje, H., Henzing, J. S., Jennings, S. G., Moerman, M., Petzold, A., Schmid, O., and Baltensperger, U.: Minimizing light absorption measurement artifacts of the Aethalometer: evaluation of five correction algorithms, *Atmos. Meas. Tech.*, 3, 457–474, <https://doi.org/10.5194/amt-3-457-2010>, 2010.
- Delene, D. J. and Ogren, J. A.: Variability of aerosol optical properties at four North American surface monitoring sites, *J. Atmos. Sci.*, 59, 1135–1150, [https://doi.org/10.1175/1520-0469\(2002\)059<1135:VOAOPA>2.0.CO;2](https://doi.org/10.1175/1520-0469(2002)059<1135:VOAOPA>2.0.CO;2), 2002.
- Dibb, J. E.: Vertical mixing above Summit, Greenland: Insights into seasonal and high frequency variability from the radionuclide tracers ^{7}Be and ^{210}Pb , *Atmos. Environ.*, 41, 5020–5030, <https://doi.org/10.1016/j.atmosenv.2006.12.005>, 2007.
- Draxler, R. R. and Hess, G. D.: An overview of the HYSPLIT_4 modelling system for trajectories, *Aust. Meteorol. Mag.*, 47, 295–308, 1998.
- Drinovec, L., Mocnik, G., Zotter, P., Prévôt, A. S. H., Ruckstuhl, C., Coz, E., Rupakheti, M., Sciare, J., Müller, T., Wiedensohler, A., and Hansen, A. D. A.: The “dual-spot” Aethalometer: an improved measurement of aerosol black carbon with real-time loading compensation, *Atmos. Meas. Tech.*, 8, 1965–1979, <https://doi.org/10.5194/amt-8-1965-2015>, 2015.
- Dubovik, O., Smirnov, A., Holben, B. N., King, M. D., Kaufman, Y. J., Eck, T. F., and Slutsker, I.: Accuracy assessments of aerosol optical properties retrieved from Aerosol Robotic Network (AERONET) Sun and sky radiance measurements, *J. Geophys. Res.*, 105, 9791–9806, <https://doi.org/10.1029/2000JD900040>, 2000.
- Eckhardt, S., Hermansen, O., Grythe, H., Fiebig, M., Stebel, K., Cassiani, M., Baecklund, A., and Stohl, A.: The influence of cruise ship emissions on air pollution in Svalbard – a harbinger of a more polluted Arctic?, *Atmos. Chem. Phys.*, 13, 8401–8409, <https://doi.org/10.5194/acp-13-8401-2013>, 2013.
- Eleftheriadis, K., Vratolis, S., and Nyeki, S.: Aerosol black carbon in the European Arctic: Measurements at Zeppelin station, Ny-Alesund, Svalbard from 1998–2007, *Geophys. Res. Lett.*, 36, 1–5, <https://doi.org/10.1029/2008GL035741>, 2009.
- Fetterer, F., Knowles, K., Meier, W., and Savoie, M.: Sea Ice Index, Version 2. Northern Hemisphere Monthly Extent Shapefiles. Boulder, Colorado USA, NSIDC: National Snow and Ice Data Center, <https://doi.org/10.7265/N5736NV7>, last access: April 2015.
- Fleming, Z. L., Monks, P. S., and Manning, A. J.: Review: Untangling the influence of air-mass history in interpreting observed atmospheric composition, *Atmos. Res.*, 104–105, 1–39, <https://doi.org/10.1016/j.atmosres.2011.09.009>, 2012.
- Freud, E., Krecji, R., Tunved, P., Leaitch, R., Nguyen, Q. T., Quynh, T., Massling, A., Skov, H., and Barrie, L.: Pan-Arctic aerosol number size distributions: seasonality and patterns, *Atmos. Chem. Phys.*, 17, 8101–8128, <https://doi.org/10.5194/acp-17-8101-2017>, 2017.
- Groves, D. G. and Francis, J. A.: Variability of the arctic atmospheric moisture budget from TOVS satellite data, *J. Geophys. Res.*, 107, 4785, <https://doi.org/10.1029/2002JD002285>, 2002.

- Hatakka, J., Aalto, T., Aaltonen, V., Aurela, M., Hakola, H., Komppula, M., Laurila, T., Lihavainen, H., Paatero, J., Salminen, K., and Viisanen, Y.: Overview of the atmospheric research activities and results at Pallas GAW station, *Boreal Environ. Res.*, 8, 365–383, 2003.
- Heintzenberg, J. H.: Size-segregated measurements of particulate elemental carbon and aerosol light absorption at remote Arctic locations, *Atmos. Environ.*, 16, 2461–2469, [https://doi.org/10.1016/0004-6981\(82\)90136-6](https://doi.org/10.1016/0004-6981(82)90136-6), 1982.
- Hirdman, D., Burkhardt, J. F., Sodemann, H., Eckhardt, S., Jefferson, A., Quinn, P. K., Sharma, S., Ström, J., and Stohl, A.: Long-term trends of black carbon and sulphate aerosol in the Arctic: changes in atmospheric transport and source region emissions, *Atmos. Chem. Phys.*, 10, 9351–9368, <https://doi.org/10.5194/acp-10-9351-2010>, 2010.
- Hopper, J. F., Worthy, D. F. J., Barrie, L. A., and Trivett, N. B. A.: Atmospheric observations of aerosol black carbon, carbon dioxide and methane in the high Arctic, *Atmos. Environ.*, 28, 3047–3054, [https://doi.org/10.1016/1352-2310\(94\)90349-2](https://doi.org/10.1016/1352-2310(94)90349-2), 1994.
- Huang, L., Gong, S. L., Sharma, S., Lavoué, D., and Jia, C. Q.: A trajectory analysis of atmospheric transport of black carbon aerosols to Canadian high Arctic in winter and spring (1990–2005), *Atmos. Chem. Phys.*, 10, 5065–5073, <https://doi.org/10.5194/acp-10-5065-2010>, 2010.
- Hyvärinen, A. P., Kolmonen, P., Kerminen, V.-M., Virkkula, A., Leiskinen, A., Komppula, M., Hatakka, J., Burkhardt, J., Stohl, A., Aalto, P., Kulmala, M., Lehtinen, K.E.J., Viisanen, Y., and Lihavainen, H.: Aerosol black carbon at five background measurement sites over Finland, a gateway to the Arctic, *Atmos. Environ.*, 45, 4042–4050, <https://doi.org/10.1016/j.atmosenv.2011.04.026>, 2011.
- Hyvärinen, A.-P., Vakkari, V., Laakso, L., Hooda, R. K., Sharma, V. P., Panwar, T. S., Beukes, J. P., van Zyl, P. G., Josipovic, M., Garland, R. M., Andreae, M. O., Pöschl, U., and Petzold, A.: Correction for a measurement artifact of the Multi-Angle Absorption Photometer (MAAP) at high black carbon mass concentration levels, *Atmos. Meas. Tech.*, 6, 81–90, <https://doi.org/10.5194/amt-6-81-2013>, 2013.
- Johannessen, O. M., Bengtsson, L., Miles, M. W., Kuzmina, S. I., Semenov, V. A., Alekseev, G. V., Nagurnyi, A. P., Zakharov, V. F., Bobylev, L. P., Pettersson, L. H., Hasselmann, K., and Cattle, H.P.: Arctic climate change: Observed and modelled temperature and sea-ice variability, *Tellus*, 56A, 328–341, <https://doi.org/10.1111/j.1600-0870.2004.00060.x>, 2004.
- Kanamitsu, M.: Description of NMC global data assimilation and forecast system, *Weather Forecast.*, 4, 335–342, [https://doi.org/10.1175/1520-0434\(1989\)004<0335:DOTNGD>2.0.CO;2](https://doi.org/10.1175/1520-0434(1989)004<0335:DOTNGD>2.0.CO;2), 1989.
- Lihavainen, H., Kerminen, V.-M., Tunved, P., Aaltonen, V., Arola, A., Hatakka, J., Hyvärinen, A., and Viisanen, Y.: Observational signature of the direct radiative effect by natural boreal forest aerosols and its relation to the corresponding first indirect effect, *J. Geophys. Res.*, 114, D20206, <https://doi.org/10.1029/2009JD012078>, 2009.
- Lihavainen, H., Hyvärinen, A., Asmi, E., Hatakka, J., and Viisanen, Y.: Long-term variability of aerosol optical properties in northern Finland, *Boreal Env. Res.*, 20, 526–541, 2015.
- Lindsay, R. W. and Zhang, J.: The thinning of Arctic sea ice, 1988–2003: Have we passed a tipping point?, *J. Climate*, 18, 4879–4894, <https://doi.org/10.1175/JCLI3587.1>, 2005.
- Liu, D., Quennhenen, B., Darbyshire, E., Allan, J. D., Williams, P. I., Taylor, J. W., Bauguitte, S. J.-B., Flynn, M. J., Lowe, D., Gallagher, M. W., Bower, K. N., Choularton, T. W., and Coe, H.: The importance of Asia as a source of black carbon to the European Arctic during springtime 2013, *Atmos. Chem. Phys.*, 15, 11537–11555, <https://doi.org/10.5194/acp-15-11537-2015>, 2015.
- Lohila, A., Penttilä, T., Jortikka, S., Aalto, T., Anttila, P., Asmi, E., Aurela, M., Hatakka, J., Hellén, H., Henttonen, H., Hänninen, P., Kilki, J., Kyllonen, K., Laurila, T., Lepistö, A., Lihavainen, H., Makkonen, U., Paatero, J., Rask, M., Sutinen, R., Tuovinen, J.-P., Vuorenmaa, J., and Viisanen, Y.: Preface to the special issue on integrated research of atmosphere, ecosystems and environment at Pallas, *Boreal Env. Res.*, 20, 431–454, 2015.
- May, N. W., Quinn, P. K., McNamara, S. M., and Pratt, K. A.: Multiyear study of the dependence of sea salt aerosol on wind speed and sea ice conditions in the coastal Arctic, *J. Geophys. Res.-Atmos.*, 121, 9208–9219, <https://doi.org/10.1002/2016JD025273>, 2016.
- Mitchell, J. M.: Visual range in the polar regions with particulate reference to the Alaskan Arctic, *J. Atmos. Terr. Phys.*, special supplement, 1, 95–211, 1957.
- Müller, T., Henzing, J. S., de Leeuw, G., Wiedensohler, A., Alastuey, A., Angelov, H., Bizjak, M., Collaud Coen, M., Engström, J. E., Gruening, C., Hillamo, R., Hoffer, A., Imre, K., Ivanow, P., Jennings, G., Sun, J. Y., Kalivitis, N., Karlsson, H., Komppula, M., Laj, P., Li, S.-M., Lunder, C., Marinoni, A., Martins dos Santos, S., Moerman, M., Nowak, A., Ogren, J. A., Petzold, A., Pichon, J. M., Rodriguez, S., Sharma, S., Sheridan, P. J., Teinalä, K., Tuch, T., Viana, M., Virkkula, A., Weingartner, E., Wilhelm, R., and Wang, Y. Q.: Characterization and intercomparison of aerosol absorption photometers: result of two intercomparison workshops, *Atmos. Meas. Tech.*, 4, 245–268, <https://doi.org/10.5194/amt-4-245-2011>, 2011.
- Najafi, M. R., Zwiers, F. W., and Gillett, N. P.: Attribution of Arctic temperature change to greenhouse-gas and aerosol influences, *Nat. Clim. Change*, 5, 246–249, <https://doi.org/10.1038/nclimate2524>, 2015.
- Ogren, J. A.: Comment on calibration and intercomparison of filter-based measurements of visible light absorption by aerosols, *Aerosol Sci. Tech.*, 44, 589–591, <https://doi.org/10.1080/02786826.2010.482111>, 2010.
- Ogren, J. A., Wendell, J., Andrews, E., and Sheridan, P. J.: Continuous light absorption photometer for long-term studies, *Atmos. Meas. Tech.*, 10, 4805–4818, <https://doi.org/10.5194/amt-10-4805-2017>, 2017.
- Pandolfi, M., Alados-Arboledas, L., Alastuey, A., Andrade, M., Angelov, C., Artiñano, B., Backman, J., Baltensperger, U., Bonasoni, P., Bukowiecki, N., Collaud Coen, M., Conil, S., Coz, E., Crenn, V., Dudoitidis, V., Ealo, M., Eleftheriadis, K., Favez, O., Fetfatzis, P., Fiebig, M., Flentje, H., Ginot, P., Gysel, M., Henzing, B., Hoffer, A., Holubova Smejkalova, A., Kalapov, I., Kalivitis, N., Kouvarakis, G., Kristensson, A., Kulmala, M., Lihavainen, H., Lunder, C., Luoma, K., Lyamani, H., Marinoni, A., Mihalopoulos, N., Moerman, M., Nicolas, J., O'Dowd, C., Petäjä, T., Petit, J.-E., Pichon, J. M., Prokopciuk, N., Putaud, J.-P., Rodríguez, S., Sciare, J., Sellegri, K., Swietlicki, E., Titos, G.

- G., Tuch, T., Tunved, P., Ulevicius, V., Vaishya, A., Vana, M., Virkkula, A., Vratolis, S., Weingartner, E., Wiedensohler, A., and Laj, P.: A European aerosol phenomenology – 6: scattering properties of atmospheric aerosol particles from 28 ACTRIS sites, *Atmos. Chem. Phys.*, 18, 7877–7911, <https://doi.org/10.5194/acp-18-7877-2018>, 2018.
- Pearson, R. G., Phillips, S. J., Loranty, M. M., Beck, P. S. A., Damoulas, T., Knight, S. J., and Goetz, S. J.: Shifts in Arctic vegetation and associated feedbacks under climate change, *Nat. Clim. Change*, 3, 673–677, <https://doi.org/10.1038/nclimate1858>, 2013.
- Petzold, A. and Schönlinner, M.: Multi-angle absorption photometry: A new method for the measurement of aerosol light absorption and atmospheric black carbon, *J. Aerosol Sci.*, 35, 421–441, <https://doi.org/10.1016/j.jaerosci.2003.09.005>, 2004.
- Petzold, A., Ogren, J. A., Fiebig, M., Laj, P., Li, S.-M., Baltensperger, U., Holzer-Popp, T., Kinne, S., Pappalardo, G., Sugimoto, N., Wehrli, C., Wiedensohler, A., and Zhang, X.-Y.: Recommendations for reporting “black carbon” measurements, *Atmos. Chem. Phys.*, 13, 8365–8379, <https://doi.org/10.5194/acp-13-8365-2013>, 2013.
- Qi, L., Li, Q., Henze, D. K., Tseng, H.-L., and He, C.: Sources of springtime surface black carbon in the Arctic: an adjoint analysis for April 2008, *Atmos. Chem. Phys.*, 17, 9697–9716, <https://doi.org/10.5194/acp-17-9697-2017>, 2017.
- Quinn, P. K., Miller, T. L., Bates, T. S., Ogren, J. A., Andrews, E., and Shaw, G. E.: A 3-year record of simultaneously measured aerosol chemical and optical properties at Barrow, Alaska, *J. Geophys. Res.*, 107, 4130, <https://doi.org/10.1029/2001JD001248>, 2002.
- Quinn, P. K., Shaw, G., Andrews, E., Dutton, E. G., Ruoho-Airola, T., and Gong, S. L.: Arctic haze: Current trends and knowledge gaps, *Tellus*, 59B, 99–114, <https://doi.org/10.1111/j.1600-0889.2006.00238.x>, 2007.
- Quinn, P. K., Bates, T. S., Baum, E., Doubleday, N., Fiore, A. M., Flanner, M., Fridlind, A., Garrett, T. J., and Koch, D.: Short-lived pollutants in the Arctic: Their climate impact and possible mitigation strategies, *Atmos. Chem. Phys.*, 8, 1723–1735, 2008.
- Quinn, P. K., Stohl, A., Arneth, A., Berntsen, T., Burkhardt, J. F., Christensen, J., Flanner, M., Kupiainen, K., Lihavainen, H., Shepherd, M., Shevchenko, V., Skov, H., and Vestreng, V.: The Impact of Black Carbon on Arctic Climate, Arctic Monitoring and Assessment Programme (AMAP), Oslo, 72 pp., 2011.
- Rahn, K. A., Boys, R. D., and Shaw, G. E.: The Asian source of Arctic haze bands, *Nature*, 268, 713–715, <https://doi.org/10.1038/268713a0>, 1977.
- Serreze, M. C. and Barry, R. G.: Processes and impacts of Arctic amplification: A research synthesis, *Global Planet Change*, 77, 85–96, <https://doi.org/10.1016/j.gloplacha.2011.03.004>, 2011.
- Serreze, M. C. and Francis, J. A.: The Arctic amplification debate, *Climate Change*, 76, 241–264, <https://doi.org/10.1007/s10584-005-9017-y>, 2006.
- Sharma, S., Brook, J. R., Cachier, H., Chow, J., Gaudenzi, A., and Lu, G.: Light absorption and thermal measurements of black carbon in different regions of Canada, *J. Geophys. Res.*, 107, 1–11, <https://doi.org/10.1029/2002JD002496>, 2002.
- Sharma, S., Lavoue, D., Cachier, H., Barrie, L. A., and Gong, S. L.: Long-term trends of the black carbon concentrations in the Canadian Arctic, *J. Geophys. Res.*, 109, D15203, <https://doi.org/10.1029/2003JD004331>, 2004.
- Sharma, S., Andrews, E., Barrie, L. A., Ogren, J. A., and Lavoue, D.: Variations and sources of the equivalent black carbon in the high Arctic revealed by long-term observations at Alert and Barrow: 1989–2003, *J. Geophys. Res.*, 111, D14208, <https://doi.org/10.1029/2005JD006581>, 2006.
- Sharma, S., Ishizawa, M., Chan, D., Lavoué, D., Andrews, E., Eleftheriadis, K., and Maksyutov, S.: 16-year simulation of Arctic black carbon: Transport, source contribution, and sensitivity analysis on deposition, *J. Geophys. Res.-Atmos.*, 118, 943–964, <https://doi.org/10.1029/2012JD017774>, 2013.
- Shaw, G. E.: The Arctic haze phenomenon, *Bull. Amer. Meteorol. Soc.*, 76, 2403–2413, [https://doi.org/10.1175/1520-0477\(1995\)076<2403:TAHP>2.0.CO;2](https://doi.org/10.1175/1520-0477(1995)076<2403:TAHP>2.0.CO;2), 1995.
- Shaw, P. M., Russell, L. M., Jefferson, A., and Quinn, P. K.: Arctic organic aerosol measurements show particles from mixed combustion in spring haze and from frost flowers in winter, *Geophys. Res. Lett.*, 37, 1–5, <https://doi.org/10.1029/2010GL042831>, 2010.
- Sherman, J. P., Sheridan, P. J., Ogren, J. A., Andrews, E., Hageman, D., Schmeisser, L., Jefferson, A., and Sharma, S.: A multi-year study of lower tropospheric aerosol variability and systematic relationships from four North American regions, *Atmos. Chem. Phys.*, 15, 12487–12517, <https://doi.org/10.5194/acp-15-12487-2015>, 2015.
- Stein, A. F., Draxler, R. R., Rolph, G. D., Stunder, J. B., Cohen, M. D., and Ngan, F.: NOAA’s HYSPLIT atmospheric transport and dispersion modeling system, *Am. Meteorol. Soc.*, 96, 2059–2078, <https://doi.org/10.1175/BAMS-D-14-00110.1>, 2015.
- Stohl, A.: Characteristics of atmospheric transport into the Arctic troposphere, *J. Geophys. Res.*, 111, D11306, <https://doi.org/10.1029/2005JD006888>, 2006a.
- Stohl, A., Andrews, E., Burkhardt, J. F., Forster, C., Herber, A., Hoch, S. W., Kowal, D., Lunder, C., Mefford, T., Ogren, J. A., Sharma, S., Spichtinger, N., Stebel, K., Stone, R., Ström, J., Tørseth, K., Wehrli, C., and Yttri, K. E.: Pan-Arctic enhancements of light absorbing aerosol concentrations due to North American boreal forest fires during summer 2004, *J. Geophys. Res.*, 111, D22214, <https://doi.org/10.1029/2006JD007216>, 2006b.
- Stohl, A., Berg, T., Burkhardt, J. F., Fjæraa, A. M., Forster, C., Herber, A., Hov, Ø., Lunder, C., McMillan, W. W., Oltmans, S., Shiobara, M., Simpson, D., Solberg, S., Stebel, K., Ström, J., Tørseth, K., Treffeisen, R., Virkkunen, K., and Yttri, K. E.: Arctic smoke – record high air pollution levels in the European Arctic due to agricultural fires in Eastern Europe in spring 2006, *Atmos. Chem. Phys.*, 7, 511–534, <https://doi.org/10.5194/acp-7-511-2007>, 2007.
- Stone, R. S., Anderson, G. P., Andrews, E., Dutton, E. G., Shettle, E. P., and Berk, A.: Incursions and radiative impact of Asian dust in northern Alaska, *Geophys. Res. Lett.*, 34, L14815, <https://doi.org/10.1029/2007GL029878>, 2007.
- Stone, R. S., Sharma, S., Herber, A., Eleftheriadis, K., and Nelson, D. W.: A characterization of Arctic aerosols on the basis of aerosol optical depth and black carbon measurements, *Elementa*, 2, 1–22, <https://doi.org/10.12952/journal.elementa.000027>, 2014.

- Stroeve, J., Holland, M. M., Meier, W., Scambos, T., and Serreze, M.: Arctic sea ice decline: Faster than forecast, *Geophys. Res. Lett.*, 34, 1–5, <https://doi.org/10.1029/2007GL029703>, 2007.
- Stroeve, J. C., Kattsov, V., Barrett, A., Serreze, M., Pavlova, T., Holland, M., and Meier, W. N.: Trends in Arctic sea ice extent from CMIP5, CMIP3 and observations, *Geophys. Res. Lett.*, 39, 1–7, <https://doi.org/10.1029/2012GL052676>, 2012.
- Ström, J., Umegård, J., Tørseth, K., Tunved, P., Hansson, H. C., Holmén, K., Wismann, V., Herber, A., and König-Langlo, G.: One year of particle size distribution and aerosol chemical composition measurements at the Zeppelin station, *Phys. Chem. Earth*, 28, 1181–1190, <https://doi.org/10.1016/j.pce.2003.08.058>, 2003.
- Toledano, C., Cachorro, V., Berjon, A., De Frutos, A., Sorribas, M., De la Morena, B., and Goloub, P.: Aerosol optical depth and Ångström exponent climatology at El Arenosillo AERONET site (Huelva, Spain), *Q. J. R. Meteorol. Soc.*, 133, 795–807, <https://doi.org/10.1002/qj.54>, 2007.
- Tunved, P., Hansson, H.-C., Kerminen, V.-M., Ström, J., Dal Maso, M., Lihavainen, H., Viisanen, Y., Aalto, P. P., Komppula, M., and Kulmala, M.: High natural aerosol loading over boreal forests, *Science*, 312, 261–263, <https://doi.org/10.1126/science.1123052>, 2006.
- Twomey, S.: The influence of pollution on the shortwave albedo of clouds, *J. Atmos. Sci.*, 34, 1149–1152, [https://doi.org/10.1175/1520-0469\(1977\)034<1149:TIOPOT>2.0.CO;2](https://doi.org/10.1175/1520-0469(1977)034<1149:TIOPOT>2.0.CO;2), 1977.
- Uttal, T., Makshtas, A., and Laurila, T.: The Tiksi International Hydrometeorological Observatory – An Arctic Members Partnership, *WMO Bulletin*, 62, 22–26, 2013.
- Uttal, T., Starkweather, S., Drummond, J. R., Vihma, T., Makshatas, A. P., Darby, L. S., Burkhardt, J. F., Cox, C. J., Schmeisser, L. N., Haiden, T., Maturilli, M., Shupe, M. D., De Boer, G., Saha, A., Grachev, A. A., Crepinsek, S. M., Bruhwiler, L., Goodison, B., McArthur, B., Walden, V. P., Dlugokencky, E. J., Persson, P. O., Lesins, G., Laurila, T., Ogren, J. A., Stone, R., Long, C. N., Sharma, S., Massling, A., Turner, D. D., Stanitski, D. M., Asmi, E., Aurela, M., Skov, H., Eleftheriadis, K., Virkkula, A., Platt, A., Førland, E. J., Iijima, Y., Nielsen, I. E., Bergin, M. H., Candalish, L., Zimov, N. S., Zimov, S. A., O'Neill, N. T., Fogal, P. F., Kivi, R., Konopleva-Akish, E. A., Verlinde, J., Kustov, V. Y., Vasel, B., Ivakhov, V. M., Viisanen, Y., and Intrieri, J. M.: International Arctic Systems for Observing the Atmosphere: An International Polar Year Legacy Consortium, *Bull. Amer. Meteor. Soc.*, 97, 1033–1056, <https://doi.org/10.1175/BAMS-D-14-00145.1>, 2016.
- VanCuren, R. A., Cahill, T., Burkhardt, J., Barnes, D., Zhao, Y., Perry, K., Cliff, S., and McConnell, J.: Aerosols and their sources at summit Greenland: First results of continuous size- and time-resolved sampling, *Atmos. Environ.*, 52, 82–97, <https://doi.org/10.1016/j.atmosenv.2011.10.047>, 2012.
- Wang, H., Rasch, P., Easter, R., Singh, B., Zhang, R., Ma, P., Qian, Y., Ghan, S., and Beagley, N.: Using an explicit emission tagging method in global modeling of source-receptor relationships for black carbon in the Arctic: Variations, sources, and transport pathways, *J. Geophys. Res.-Atmos.*, 119, 1–22, <https://doi.org/10.1002/2014JD022297>, 2014.
- Wang, M. and Overland, J. E.: Detecting Arctic climate change using Köppen climate classification, *Climate Change*, 67, 43–62, <https://doi.org/10.1007/s10584-004-4786-2>, 2004.
- Wiscombe, W. J. and Grams, G. W.: The backscattered fraction in two-stream approximations, *J. Atmos. Sci.*, 33, 2440–2451, 1976.

© 2018. This work is published under
<https://creativecommons.org/licenses/by/4.0/> (the “License”). Notwithstanding
the ProQuest Terms and Conditions, you may use this content in accordance
with the terms of the License.